THE UNIVERSITY OF ALBERTA

THE EFFECT OF A SURFACE COVER ON OPEN CHANNEL SURGES

by

RICHARD HAMILTON COOPER

A THESIS

SUBMITTED TO THE FACULTY OF GRADUATE STUDIES

IN PARTIAL FULFILMENT OF THE REQUIREMENTS FOR THE DEGREE OF

MASTER OF SCIENCE

DEPARTMENT OF CIVIL ENGINEERING

EDMONTON, ALBERTA

May 1966

UNIVERSITY OF ALBERTA

FACULTY OF GRADUATE STUDIES

The undersigned certify that they have read, and recommend to the Faculty of Graduate Studies for acceptance, a thesis entitled

THE EFFECT OF A SURFACE COVER

ON OPEN CHANNEL SURGES

submitted by Richard Hamilton Cooper in partial fulfilment of the requirements for the degree of Master of Science.

ABSTRACT

This thesis summarizes an investigation on the effect of a surface cover on open channel surges. Data are reported for an experimental study utilizing an artificial surface cover having continuity and structural strength. A novel surge recording system comprised of a number of pressure transducers coupled to an X-Y recorder was used in the experiments.

A functional relationship between Froude number based on velocity of propagation $V_w/\sqrt{gy_o}$ and non-dimensional surge height η/y_o is suggested from dimensional considerations and from open water surge theory. This relationship is confirmed experimentally for surface cover conditions and is found to be independent of surface cover properties over the range of testing.

A radical change in the profile of a surge is observed to occur with the addition of a surface cover.

ACKNOWLEDGEMENTS

The author wishes to extend his appreciation to Professor J. P. Verschuren for his guidance and constructive criticism rendered throughout the project.

Professor A. W. Peterson along with the staff of the Hydraulics Laboratory gave valuable assistance in the design and construction of the experimental apparatus. Special thanks are due to Mr. G. Shook, who designed, modified and operated the surge recording system.

TABLE OF CONTENTS

	Page
TITLE PAGE	i
APPROVAL SHEET	ii
ABSTRACT	iii
ACKNOWLEDGEMENTS	iv
TABLE OF CONTENTS	v
LIST OF TABLES	vii
LIST OF FIGURES	viii
LIST OF PLATES	x
GLOSSARY OF SYMBOLS	xi
CHAPTER	
I INTRODUCTION	
The Problem	1
Purpose and Scope	2
Historical Review	3
II THEORETICAL ASPECTS OF OPEN CHANNEL SURGES	
General	7
Theoretical and Physical Aspects of an Open Channel Surge for Open-Water Conditions	7
Celerity Equation for a Steep-Fronted Surge	11
Modification of the Celerity Equation for Surface Cover Conditions	13
Dimensional Aspects	17
III THE EXPERIMENTAL PROGRAM	
General	20
Experimental Apparatus	20
Surge Recording System	25
Artificial Surface Covers	30
Calibration of the Recording System	36
Experimental Procedure	36

CHAPTER		Page
IV	EXPERIMENTAL RESULTS	
	General	39
	Surge Height-Velocity Relationship for Open-Water Conditions	40
	Surge Height-Velocity Relationship for Surface Cover Conditions . . .	44
	Surface Profiles	51
V	DISCUSSION OF RESULTS	
	General	57
	Open-Water Surges	57
	Surface Profiles for Surges Observed Under Surface Cover Conditions . .	59
	Surge Height-Velocity Relationship for Surface Cover Conditions . . .	62
VI	CONCLUSIONS AND RECOMMENDATIONS	
	Conclusions	68
	Recommendations	69
LIST OF REFERENCES	. . . .	71
APPENDIX		
"A"	- DATA PROCESSING	A-1
"B"	- THE PROCESSED DATA	B-1

LIST OF TABLES

Table		Page
III-1	Surface Cover Properties	35
IV-1	Index of Processed Data	41
IV-2	Regression Analysis Results	50
B -1	Processed Data - No Surface Cover .	B-2
B -2	Processed Data - Cover No. 1 . . .	B-4
B -3	Processed Data - Cover No. 2 . . .	B-6
B -4	Processed Data - Cover No. 3 . . .	B-8
B -5	Processed Data - Cover No. 4 . . .	B-10
B -6	Processed Data - Cover No. 5 . . .	B-12

LIST OF FIGURES

Figure		Page
II-1	Types of Surge-Wave Profiles	9
II-2	Surge Height-Velocity Relationship for Undular Open-Water Surges	12
II-3	Open Channel Surge with Surface Cover . .	14
III-1	Experimental Apparatus - Schematic Drawing	22
III-2	Pressure Transducer System - Schematic Drawing	26
III-3	Typical Cover Connection	32
III-4	Typical Surge Records	38
IV-1	Maximum Surge Height-Velocity Relationship for No Surface Cover	42
IV-2	Average Surge Height-Velocity Relationship for No Surface Cover . .	43
IV-3	Average Surge Height-Velocity Relationship for Cover No. 1	45
IV-4	Average Surge Height-Velocity Relationship for Cover No. 2	46
IV-5	Average Surge Height-Velocity Relationship for Cover No. 3	47
IV-6	Average Surge Height-Velocity Relationship for Cover No. 4	48
IV-7	Average Surge Height-Velocity Relationship for Cover No. 5	49

Figure		Page
IV-8	Surface Profiles for Open-Water Surges	53
IV-9 IV-10	Surface Profiles for Different Cover Conditions	54
IV-11	Surface Profiles - Range of Froude Numbers	56
V-1	Typical Surface Profile - Surface Cover Conditions	60
V-2	Summary of Surge Height-Velocity Relationship Results	66

LIST OF PLATES

Plate		Page
III-1	Entrance tank and valves	24
III-2	Test flume	24
III-3	Transducer assembly and driver unit .	28
III-4	X-Y Recorder and control section . .	28
III-5	Cover 1	33
III-6	Cover 2	33
III-7	Cover 3	34
III-8	Cover 4	34

GLOSSARY OF SYMBOLS

a - Vertical distance from the undisturbed level to the free water surface.

b - Breadth of the flume.

c - Parameter defined by Equation 1-1.

C - Celerity.

E_i - Modulus of elasticity of surface cover.

g - Acceleration due to gravity.

h_i - Thickness of surface cover.

h_s - Submerged thickness of surface cover.

L - Distance measured on surge records representing the time required for the toe of a surge to travel the distance between recording stations.

Q - Discharge.

V_w - Velocity of propagation of the toe of a surge in space.

V - Mean velocity of flow.

δV - Change in mean velocity of flow over a surge.

y_p - Undisturbed piezometric depth.

y_o - Undisturbed depth of water.

y_1 - Uniform depth of water behind a surge.

γ_i - Unit weight of surface cover.

γ_w - Unit weight of water.

ϵ - Roughness height of flume.

ϵ_i - Roughness height of surface cover.

η - Theoretical surge height.

η_{ave} - Average surge height.

η_{max} - Maximum surge height.

λ - Wavelength.

μ - Dynamic viscosity of water.

ρ_i - Mass density of surface cover.

ρ_w - Mass density of water.

ω - Time frequency of waves.

CHAPTER I

INTRODUCTION

1.1 The Problem

The operation of dams on northern rivers usually involves the periodic release of large quantities of water for winter flow regulation and for the generation of hydroelectric power. This rapid change in flow causes a surge to form and propagate through the channel downstream from the dam. In the past a considerable amount of work has been done to analyse the behavior of such a surge and several comprehensive works have been written (Lamb, 1945; Keulegan, 1949; Stoker, 1957). Unfortunately, all of the theory and the resulting engineering methods are restricted in that they apply only to water having a free surface condition. In northern climates this condition is usually not satisfied during winter months when rivers and streams are covered with ice having appreciable thickness and structural strength. To date there has been no attempt made to assess the effect of a surface ice cover on an open channel surge.

This problem was recently demonstrated to engineers associated with the Brazeau project in Alberta, where plans ultimately called for releases of water during winter when

ice is present, that would be several times as large as the base flow in the river. The lack of knowledge on the behavior of a surge caused by such a release, under ice conditions, has led to the present investigation.

1.2 Purpose and Scope

The purpose of this investigation was to initiate a study into the effect of a surface ice cover, having continuity and structural strength, on the behavior of open channel surges. The main objectives of the investigation were:

1. To determine experimentally the importance of each of the variables imposed on the problem by the addition of an ice cover.
2. To determine, if possible, the manner in which the important variables affect the phenomena.
3. To physically describe the behavior of an open channel surge for surface cover conditions.

The scope of the investigation was limited by the necessity of having to use an artificial material to simulate a surface ice cover. However, the material selected for this purpose formed a continuous surface cover having structural strength. The surface roughness, rigidity and weight were independently varied throughout the testing program in an attempt to assess the importance of each of these cover properties.

The test work consisted of initiating flow at one end of a level flume containing still water and observing the resulting surge as it propagated through the channel. Although the testing apparatus was originally designed to accommodate tests for the initial condition of steady uniform flow in the flume, it was found that the recording system would require further development before reliable data could be obtained for this condition. Therefore, testing was limited to observations made on surges propagating through initially still water in a level flume.

Tests were conducted for the free surface condition and for a total of five surface covers having different values of rigidity, surface roughness and weight. Depth and discharge were varied for tests conducted under each cover condition.

1.3 Historical Review

A review of the literature indicates that all previous work associated with the problem of this investigation has been limited to a number of studies on the propagation of ocean waves and swell through fields of loose pack ice.

A theoretical study on the effect of loose pack ice on waves entering a field of such ice was made by Peters (1950). In this study the waves were assumed to

have a sinusoidal form in the free surface some distance from the edge of the icefield. The icefield was assumed to be an unconsolidated floating mat consisting of small particles that do not interact. The results of this study indicated that the effect of the mat depends on the expression:

$$c = \frac{\gamma_w}{\rho_i \omega^2 h_i - \gamma_w} \quad \ldots\ldots\ldots\ldots\ldots\ldots\ldots \quad (1\text{-}1)$$

where γ_w is the unit weight of water, ρ_i is the mass density of the floating material, h_i is the thickness of this material and ω is the time frequency. If $c > 0$ the disturbance approaching the mat is not propagated to any great distance inside the mat. If $c = 0$ the situation is similar to that of waves approaching a perfectly rigid mat and if $c < 0$ the waves pass into the mat with an altered wavelength and amplitude which are functions of $|c|$.

Since 1950, there have been several theoretical studies extending the work of Peters (Weitz and Keller, 1950; Shapiro and Simpson, 1953; Keller and Goldstein, 1953). However, each of these studies has been based on the unrealistic assumption that the ice cover is an unconsolidated floating mat.

A mathematical investigation by Krylov (1948)[1] on

[1]Taken from the Bibliography on Snow, Ice, and Permafrost. SIPRE Report 12, vol. VI, n. 7155, Snow, Ice, and Permafrost Research Establishment, U. S. Army, Corps of Engineers, Wilmette, Ill.

the propagation of long waves under ice showed that the existance of an ice cover reduces the speed of wave propagation and that the decrease is greater for higher frequency waves.

Robin (1963) conducted an experimental study on the penetration of sea waves and swell into fields of loose pack ice by means of a ship borne wave recorder. Observations were made of the amplitude and period of waves having periods ranging from 4 to 24 seconds. The diameter and thickness of the individual ice floes were also recorded. Robin concluded that the penetration of long waves, with periods from 11 to 24 seconds, into ice fields made up of large individual floes having diameters greater than half a wavelength takes place by bending of the individual floes. For shorter waves having periods between 4 and 11 seconds and floes of about 40 meters diameter and 1.5 meters thickness, penetration takes place with the individual floes behaving as rigid floating plates. A discussion of the energy required to bend large ice floes indicated that long period waves propagated through regions covered by pack ice with little loss of energy only when the energy required to bend the floes is at least an order of magnitude smaller than the total energy of the waves.

The theoretical work to date has been restricted to a study of the effect of an unconsolidated floating mat on an assumed waveform having a known velocity potential.

Similarly, the experimental work has been limited to observations of waves in fields of loose pack ice although this work considers the bending of the individual floes. Unfortunately, this work is of little value in determining the effect of a continuous ice cover having structural strength on the type of disturbance caused by a rapid variation in open channel discharge.

CHAPTER II

THEORETICAL ASPECTS OF OPEN CHANNEL SURGES

2.1 General

This chapter briefly summarizes the theory describing the behavior of an open channel surge for open water conditions and examines some theoretical aspects of the surface cover problem. The celerity equation for a steep fronted surge has been modified to apply to a simplified surface cover condition. The dimensional aspects of the surge problem for surface cover conditions have been examined as a possible approach to the analysis of experimental data.

2.2 Theoretical and Physical Aspects of an Open Channel Surge for Open-Water Conditions

If flow is rapidly varied at some point in a channel, a disturbance is created that tends to propagate away from the point where it originated. This disturbance is often referred to as a surge wave whose properties depend upon the type and magnitude of the flow change as well as certain channel properties.

The present study has been restricted to the type of surge that is formed by initiating flow at one end of a flume containing still water of uniform depth. For the

free surface condition, this type of surge assumes a constant form that travels down the flume without change of shape, but with a steadily decreasing amplitude caused by the effects of friction and ponding. For relatively small discharges, a surge takes on the undular profile shown in FIG. II-1(a). As discharge exceeds a certain limiting value, the front undulation reaches a maximum height and begins to break, resulting in the breaking undular profile of FIG. II-1(b). For even greater discharges, the profile resembles that of the classical steep fronted surge shown in FIG. II-1(c). The discharge at which the transition from one form to another takes place depends on the dimensions, shape and roughness of the flume.

The behavior of these surges, for open-water conditions, has been the subject of a number of previous studies (Favre, 1935; Benjamin and Lighthill, 1954; Sandover and Zienkiewicz, 1957). However, it is desirable to give a brief account of the theory of long waves in shallow water before reviewing the results of these studies.

Airy, in 1845, showed that the velocity of propagation relative to the undisturbed flow, for a progressive wave assumed to travel without change of form, is approximately (Lamb, 1945 art. 175):

$$\sqrt{gy_o}\left(1 + \frac{3}{2}\frac{a}{y_o}\right) \qquad \text{(2-1)}$$

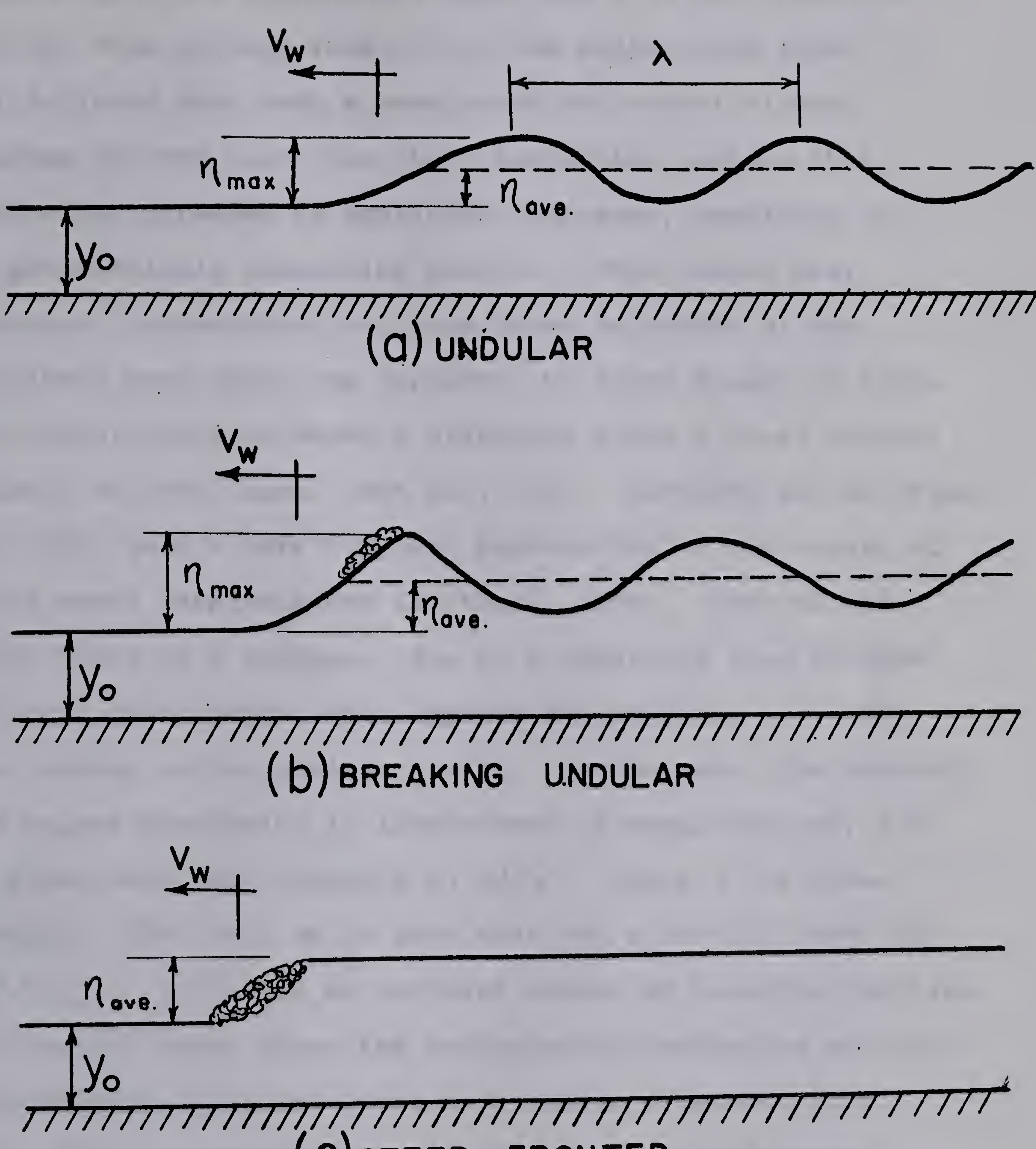

TYPES OF SURGE-WAVE PROFILES

FIGURE II-1

where y_o is the undisturbed depth and a is the elevation of the free surface relative to the undisturbed level. It followed that such a wave could not travel without change of form since the above expression implies that velocity increases as amplitude increases, resulting in a progressively steepening profile. This theory was, however, inconsistent with the known existence of the solitary wave which was observed, by Scott Russel in 1844, to travel for considerable distances along a canal without change of form (Lamb, 1945 art. 252). Korteweg and de Vries, in 1895, gave a more complete explanation of the nature of long waves (Benjamin and Lighthill, 1954). They showed that there is a tendency, due to a departure from uniform velocity with depth, that opposes the tendency of a wave to steepen corresponding to a/y_o. Furthermore, the tendency to oppose steepening is independent of amplitude and, for a given wave form, depends on y_o^2/λ^2 where λ is wave-length. They went on to show that for a certain range of $a\lambda^2/y_o^3$ there are an infinite number of possible profiles, of cnoidal form, where the two opposing tendencies exactly cancel each other resulting in a stable permanent form. As $a\lambda^2/y_o^3$ exceeds this range, the tendency to steepen dominates and the steep fronted breaking form develops.

The undular form of FIG. II-1(a) has been observed by Favre (1935) to occur in weak surges having Froude numbers based on surge velocity $V_w/\sqrt{gy_o}$ less than 1.25,

where V_w is the velocity of propagation of the surge in space[1]. The experimental results obtained by Sandover and Zienkiewicz (1957) indicate that the transition to the undular breaking form takes place at a Froude number of 1.23. These results for the surge height-velocity relationship are shown in FIG. II-2. Benjamin and Lighthill (1954) have shown that a stable undular surge profile is theoretically possible and that the wave train making up this profile has the cnoidal form.

2.3 Celerity Equation for a Steep-Fronted Surge

The classical theory for a steep fronted surge or bore, as given by Lamb (1945, art. 187), is based on the principles of continuity of mass and rate of change of momentum. For a surge travelling into initially still water with a velocity of propagation in space V_w, the motion is made steady by imposing the velocity - V_w on every particle thereby bringing the surge to rest; the celerity equation can then be deduced as:

$$V_w = \sqrt{\frac{g y_1 (y_o + y_1)}{2 y_o}} \quad \ldots\ldots\ldots\ldots\ldots\ldots \quad (2\text{-}2)$$

[1]For the case of initially still water the velocity of propagation in space or surge velocity V_w is equal to the velocity of propagation relative to the undisturbed motion or celerity C. However, for the case of an initial uniform flow with a particle velocity V_1, the velocity of propagation in space becomes:

$$V_w = C + V_1$$

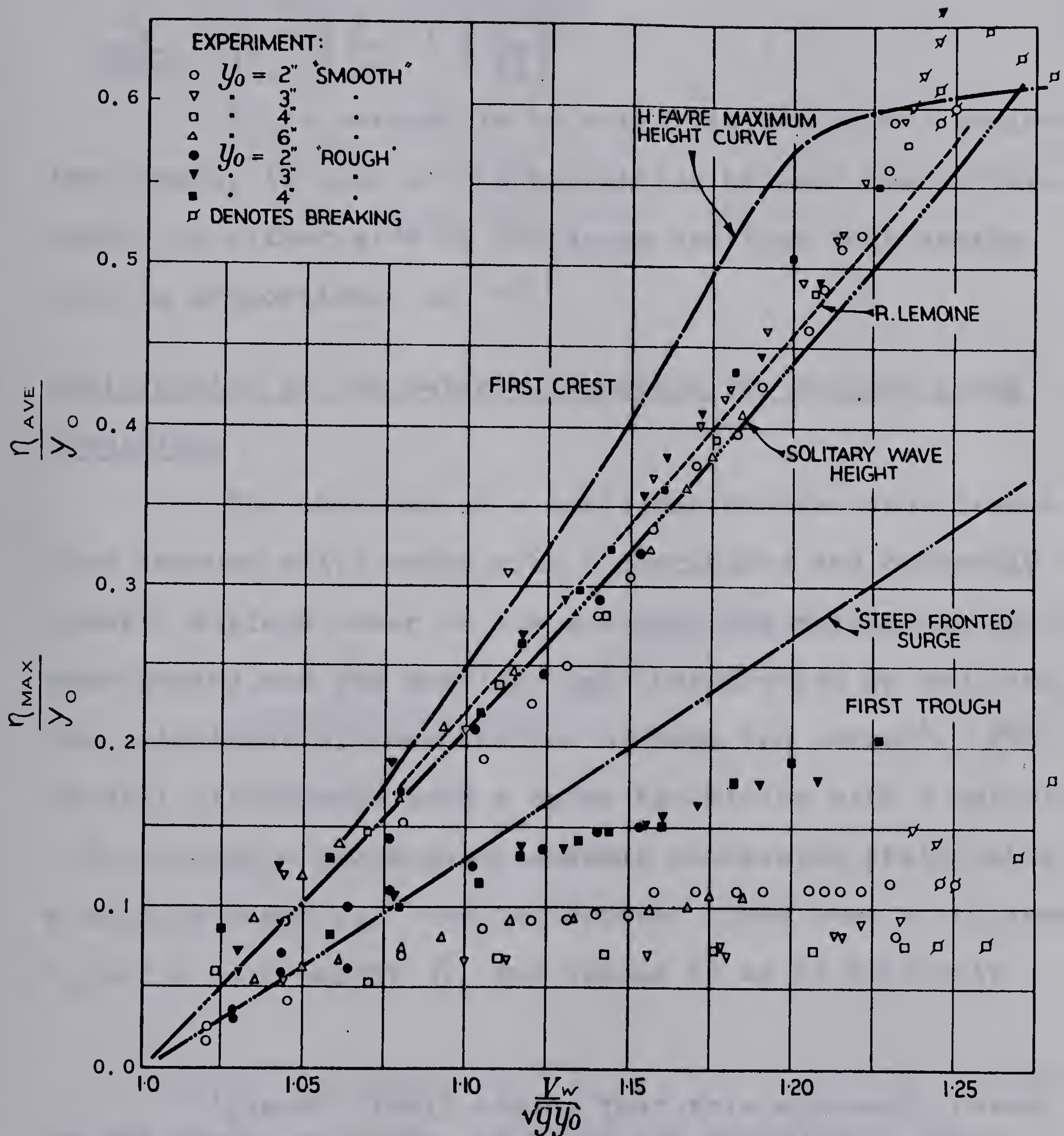

SURGE HEIGHT – VELOCITY RELATIONSHIP

FIGURE II–2

[FROM SANDOVER AND ZIENKIEWICZ, 1957]

where y_o is the depth of the still water and y_1 is the uniform depth after the surge passes. By substituting $(\eta + y_o)$ for y_1, where η is the surge height, and simplifying, Equation (2-2) becomes:

$$\frac{V_w}{\sqrt{gy_o}} = \left(1 + \frac{3}{2}\frac{\eta}{y_o} + \frac{1}{2}\frac{\eta^2}{y_o^2}\right)^{1/2} \quad \text{. . . . .} \quad (2\text{-}3)$$

It is worthwhile to note that the theory indicates that energy is lost at the transition between the uniform depths on either side of the surge and that this energy loss is proportional to η^3.

2.4 Modification of the Celerity Equation for Surface Cover Conditions

For the case of a small but finite surge travelling through still water with a continuous and perfectly elastic surface cover on its surface, the motion can be made steady and the problem then investigated by applying the principles of conservation of mass and energy[1]. FIG. II-3(a) illustrates such a surge travelling with a velocity $-V_w$ through a rectangular channel containing still water at a uniform depth y_o. Let the surface cover have a thickness h_i and a unit weight γ_i and assume it to be perfectly

[1]Blench (1961) argues that this approach, based on the energy equation, is valid for vanishingly small surges since loss of energy is proportional to the third power of amplitude and therefore vanishes in the limit.

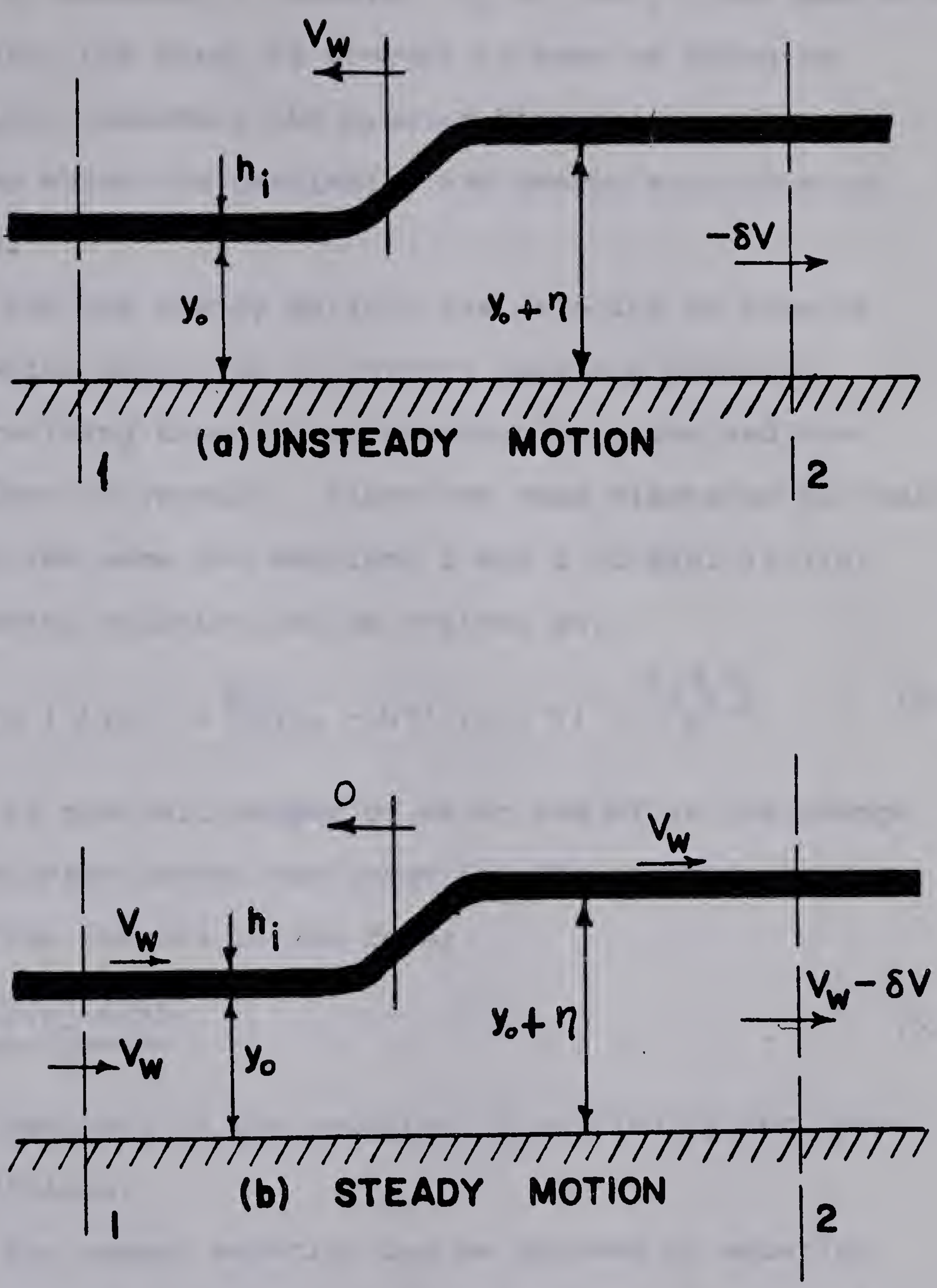

OPEN CHANNEL SURGE WITH SURFACE COVER

FIGURE II-3

elastic. By imposing a velocity $+V_w$ on every fluid particle and boundary, the surge is brought to rest as shown in FIG. II-3(b), therefore the problem becomes one of steady motion from which the continuity and energy equations can be derived.

For the steady motion, the velocity of flow in the horizontal direction is uniform over any vertical section providing there is no boundary friction and the surface slope is gradual. Since the mass discharge per unit breadth is the same for sections 1 and 2 of FIG. II-3(b), the continuity equation can be written as:

$$\frac{V_w}{g}(\gamma_w y_o + \gamma_i h_i) = \frac{\gamma_w}{g}(V_w - \delta V)(y_o + \eta) + \frac{V_w \gamma_i h_i}{g} \quad . \; . \qquad (2\text{-}4)$$

where γ_w is the unit weight of water and δV is the change in flow velocity across the surge for the unsteady motion. This equation reduces to the form:

$$V_w = \frac{\delta V(y_o + \eta)}{\eta} \quad . \; . \; . \; . \; . \; . \; . \; . \; . \; . \; . \; . \; . \; . \; . \; . \; . \; . \; . \qquad (2\text{-}5)$$

which is identical to the equation of continuity for open water conditions.

The energy equation can be derived by equating the expression for the energy of the motion of section 1 of FIG. II-3(b) to the similar expression for the motion at section 2, providing the rate at which energy lost in the motion between these sections is negligible. For the assumed perfectly elastic cover, the rate of dissipation

of energy due to bending is zero since the energy required to bend the cover is recovered when the cover becomes straight at the higher level. Furthermore, for small surge heights the loss of energy due to internal friction can be taken as negligible since this loss is proportional to the third power of surge height. Therefore, if boundary shear stresses are assumed to be zero as in the case of a frictionless fluid, the rate of work done by these shear stresses is zero and the total loss of energy in the steady motion between sections 1 and 2 can be assumed negligible.

In calculating the energy of motion it is necessary to consider the energy of the surface cover as well as the fluid, since the surface cover forms a part of the motion. Thus, by equating the total energies of motion per unit weight of fluid flowing at sections 1 and 2, we obtain:

$$y_o + \frac{V_w^2}{2g} + \frac{V_w h_i \gamma_i}{V_w y_o \gamma_w}\left(y_o + \frac{h_i}{2} + \frac{V_w^2}{2g}\right)$$

$$= y_o + \eta + \frac{(V_w - \delta V)^2}{2g} + \frac{V_w h_i \gamma_i}{V_w y_o \gamma_w}\left(y_o + \eta + \frac{h_i}{2} + \frac{V_w^2}{2g}\right). \quad (2\text{-}6)$$

which simplifies to:

$$\frac{\delta V V_w}{g} - \frac{\delta V^2}{2g} = \eta\left(1 + \frac{h_i \gamma_i}{y_o \gamma_w}\right) \quad . . . . \quad (2\text{-}7)$$

By substituting for δV from Equation (2-5), we obtain:

$$\frac{V_w^2}{g}\left(\frac{\eta}{y_o + \eta}\right) - \frac{V_w^2}{2g}\left(\frac{\eta}{y_o - \eta}\right)^2 = \eta\left(1 + \frac{h_i \gamma_i}{y_o \gamma_w}\right) \quad . . . . . . \quad (2\text{-}8)$$

which can be rearranged as:

$$V_w^2 = g\left(\frac{\eta(1 + h_i\gamma_i/y_o\gamma_w)}{\eta/(y_o + \eta) - \frac{1}{2}(\eta/(y_o + \eta))^2}\right)$$

$$= g\left(\frac{y_o + \eta}{1 - \eta/2(y_o + \eta)}\right)\left(1 + \frac{h_i\gamma_i}{y_o\gamma_w}\right)$$

$$= gy_o\left(1 + \frac{\eta}{y_o}\right)\left(\frac{1}{1 - \eta/2(y_o + \eta)}\right)\left(1 + \frac{h_i\gamma_i}{y_o\gamma_w}\right) \quad . . . \; (2\text{-}9)$$

Now, if η is small:

$$\frac{1}{1 - \eta/2(y_o + \eta)} \approx \frac{1}{1 - \eta/2y_o} = \frac{1 + \eta/2y_o}{1 - \eta^2/4y_o^2} \approx 1 + \frac{\eta}{2y_o}$$

Therefore, Equation (2-9) becomes:

$$V_w^2 = gy_o\left(1 + \frac{\eta}{y_o}\right)\left(1 + \frac{\eta}{2y_o}\right)\left(1 + \frac{h_i\gamma_i}{y_o\gamma_w}\right) \quad . . . . . \; (2\text{-}10)$$

which can be rearranged as:

$$\frac{V_w}{\sqrt{gy_o}} = \left(1 + \frac{3}{2}\frac{\eta}{y_o} + \frac{1}{2}\frac{\eta^2}{y_o^2}\right)^{\frac{1}{2}}\left(1 + \frac{h_i\gamma_i}{y_o\gamma_w}\right)^{\frac{1}{2}} \quad . . . . \; (2\text{-}11)$$

For the free surface case $\left(1 + \gamma_i h_i/y_o\gamma_w\right) = 1.0$ and Equation (2-11) is identical to the celerity equation for a steep fronted open water surge (Equation 2-3).

2.5 Dimensional Aspects

A further understanding can possibly be obtained by examining the problem from a dimensional viewpoint. The standard dimensional analysis is performed by expressing the problem as a functional equation in terms of all the

interrelated variables thought to be important and then forming standard non-dimensional parameters from these variables.

Suppose that water, with viscosity μ and mass density ρ_w, lies at rest at a uniform depth y_o in a flume having a mean surface roughness height ϵ and a breadth b. Furthermore, let the water have on its surface a continuous cover having a density ρ_i, a thickness h_i, a surface roughness height ϵ_i and a modulus of elasticity E_i. If it is accepted that the motion due to gravity g, that results from initiating a flow Q at one end of this flume is completely determined by the above variables, then the problem can be expressed in functional form as:

$$\eta, V_w, \ldots = fn(Q, g, y_o, \rho_w, \mu, \epsilon, b, \rho_i, h_i, \epsilon_i, E_i) \quad . \; . \; . \; . \quad (2\text{-}12)$$

By interchanging η with Q and forming non-dimensional parameters, we obtain the following functional equation in non-dimensional form.

$$\frac{V_w}{\sqrt{gy_o}} = fn\left(\frac{\eta}{y_o}, \frac{h_i}{y_o}, \frac{\epsilon_i}{y_o}, \frac{\rho_i}{\rho_w}, \frac{E_i/\rho_i}{gy_o}, \frac{V_w \rho_w y_o}{\mu}, \frac{b}{y_o}, \frac{\epsilon}{y_o}\right) \quad . \; . \quad (2\text{-}13)$$

In this equation; h_i/y_o, ϵ_i/y_o, ρ_i/ρ_w and $E_i/\rho_i g y_o$ are the parameters that have been formed by the variables imposed on the problem by the addition of a surface cover. Experimental and theoretical evidence for open water surges (FIG. II-2 and Equation 2.3) show a relationship between $V_w/\sqrt{gy_o}$ and η/y_o that is independent of the non-dimensional groups $V_w \rho_w y_o/\mu$, b/y_o and ϵ/y_o. Therefore,

for the open water case, Equation (2-13) reduces to:

$$\frac{V_w}{\sqrt{gy_o}} = fn\left(\frac{\eta}{y_o}\right) \quad \ldots\ldots\ldots\ldots\ldots\ldots \quad (2\text{-}14)$$

This implies that for surface cover conditions, Equation (2-13) can be simplified to the form:

$$\frac{V_w}{\sqrt{gy_o}} = fn\left(\frac{\eta}{y_o}, \frac{h_i}{y_o}, \frac{\epsilon_i}{y_o}, \frac{\rho_i}{\rho_w}, \frac{E_i/\rho_i}{gy_o}\right) \quad \ldots\ldots\ldots\ldots \quad (2\text{-}15)$$

assuming that the addition of a cover does not cause the non-dimensional groups $V_w\rho_w y_o/\mu$, b/y_o and ϵ/y_o to become important. One method of analyzing this problem would then be to assess the importance of the groups imposed by the addition of a cover on the relationship between $V_w/\sqrt{gy_o}$ and η/y_o.

CHAPTER III

THE EXPERIMENTAL PROGRAM

3.1 General

A testing program was conducted in the hydraulics laboratory at the University of Alberta. The tests consisted of initiating flow at one end of a rectangular flume containing still water and observing the change in surface elevation of the resulting surge as it passed by each of several recording stations located along the flume. Undisturbed depth and supply discharge were also measured.

Tests were conducted for six surface covers and for the free surface condition. For each surface condition, tests were run at undisturbed piezometric depths of 0.2, 0.3 and 0.4 ft., where piezometric depth is the depth measured from the free water surface to the floor of the flume and is greater than the undisturbed depth by an amount equal to the submerged thickness of the surface cover. The supply discharge was varied between tests conducted at each depth.

3.2 Experimental Apparatus

In designing the testing apparatus the main objective was to provide a system whereby surges could be produced in a flume containing water either at rest or in an initial state of steady uniform motion. Although

the equipment was originally designed and constructed to accommodate both of these initial conditions, the testing program was restricted to tests conducted for initially still water at a uniform depth (see Sect. 1.2). A number of features incorporated in the design were adapted from a test unit used by Sandover and Zienkiewicz (1957) for their experiments on undular surge waves.

FIG. III-1 shows a schematic drawing of the testing apparatus. Exclusive of instrumentation it consists of a rectangular flume, entrance and discharge tanks and a constant head surge tank. The system was non-circulating as water was supplied from the water distribution system of the City of Edmonton and was discharged into the laboratory sump.

The constant head surge tank was constructed of steel and was rectangular in shape. It contained a number of rectangular weirs that allowed excess supply to overflow and return to the laboratory sump thereby maintaining a constant head in the tank. The surge tank received a constant supply of 0.5 cfs. which was, therefore, the maximum supply discharge to the flume.

Piping from the surge tank to the flume consisted of a section of 4 in. plastic pipe running down, from the tank to the floor, and a section of 4 in. aluminum pipe running from there to the entrance tank. The aluminum section contained an orifice fitting for flow measurement,

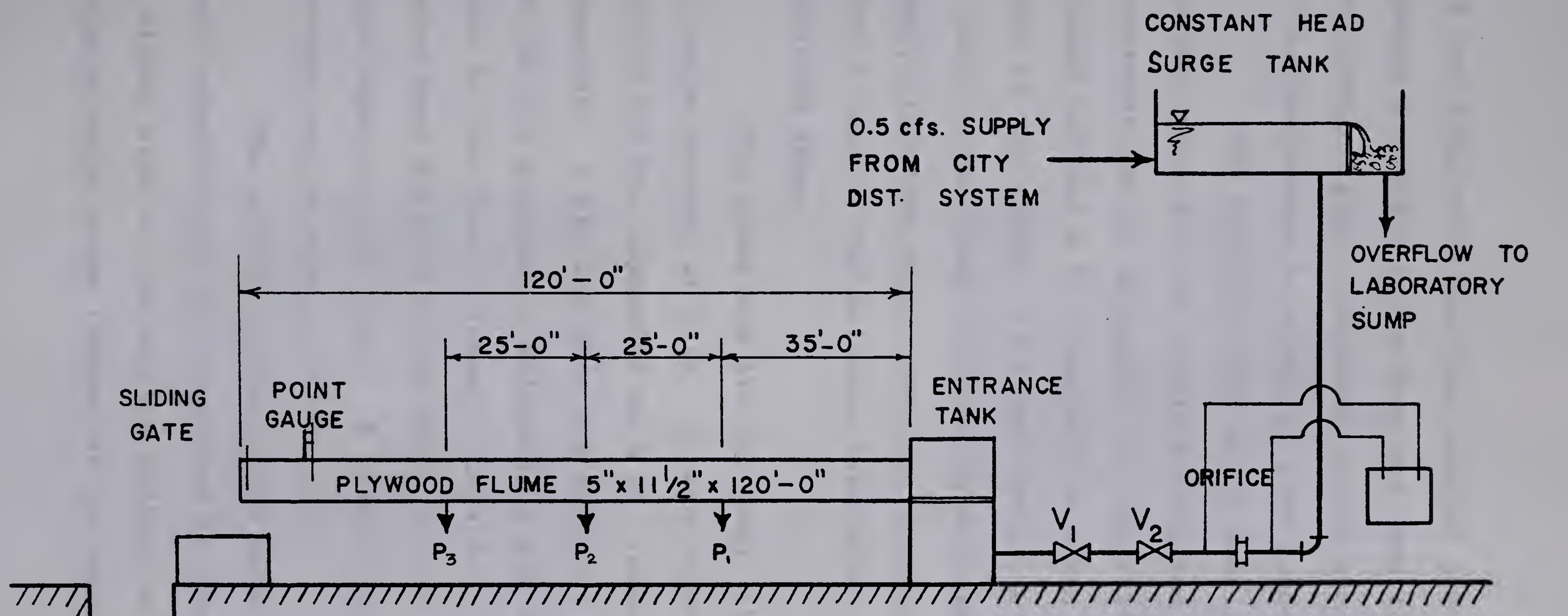

NOTES:

- P_1, P_2, P_3, INDICATE THE LOCATION OF PRESSURE TRANSDUCER TAPS
- V_1 IS A 4'' DIA. QUICK OPENING BUTTERFLY VALVE.
- V_2 IS A 4'' DIA. PLUG VALVE.

EXPERIMENTAL EQUIPMENT —— SCHEMATIC DRAWING

FIGURE III-1

FIGURE III-1

EXPERIMENTAL EQUIPMENT — SCHEMATIC DIAGRAM

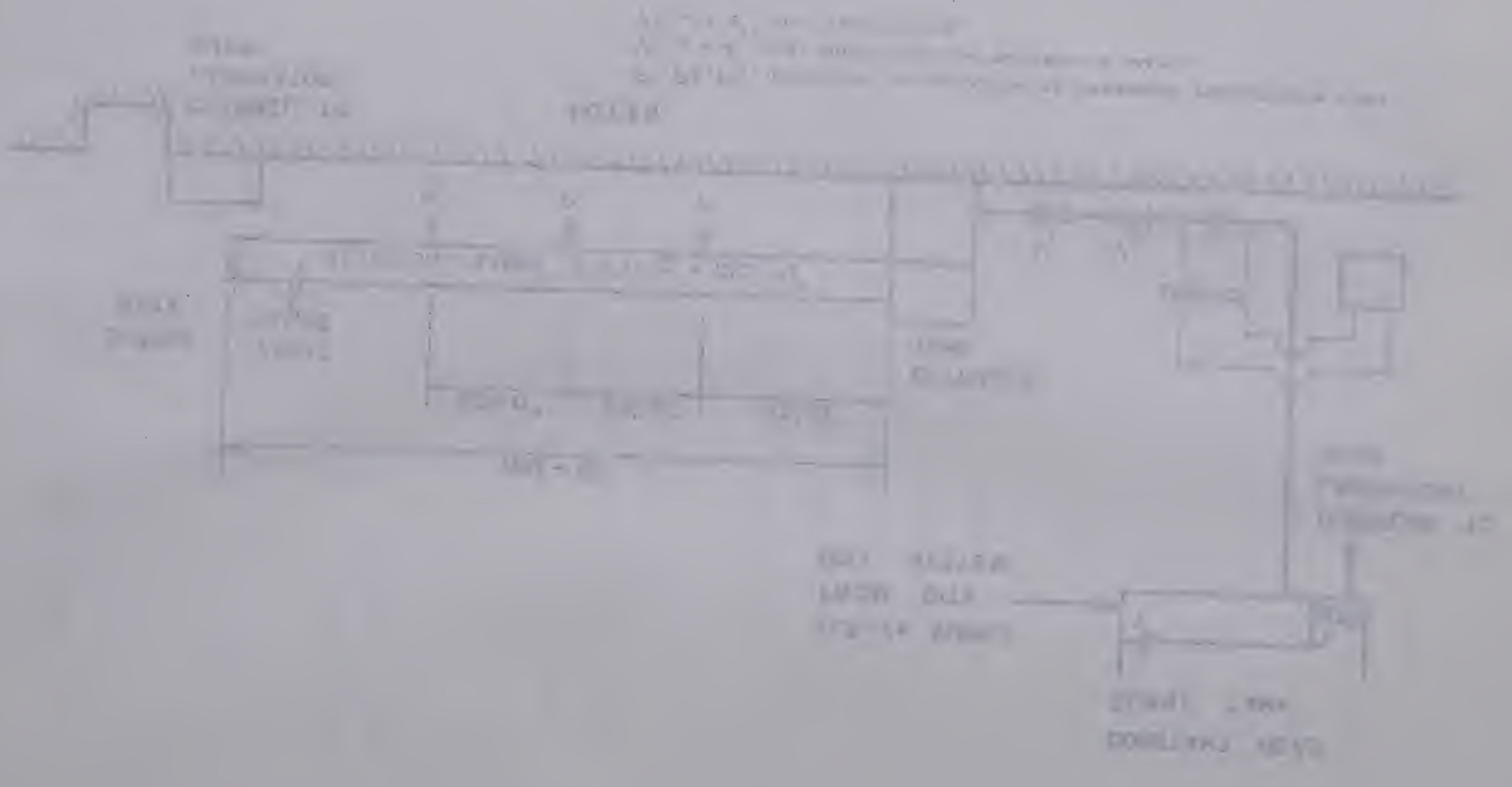

a 4 in. plug valve for flow control and a 4 in. quick opening butterfly valve that was used to initiate flow. The aluminum pipe terminated inside the entrance tank where it was perforated to minimize flow concentrations.

The entrance tank was primarily designed to provide space for the supply piping and to reduce flow concentrations on entrance. It was built of ¾ in. fir-plywood and was 4 ft. long with a width of 3 ft. below the floor of the flume. At flume level, the width was reduced to that of the flume in order to minimize the portion of supply discharge going into tank storage. PLATE III-1 shows a view of the entrance tank along with the two valves mentioned above.

The flume was 120 ft. long, 11½ in. deep and had an inside breadth of 5 in. It was constructed from fir-plywood and was supported at 8 ft. intervals by dexion framework. A sliding gate was built at the downstream end for the purpose of maintaining the desired still water depth in the flume. Pressure taps for the surge recording system were drilled in the floor of the flume at the locations shown in FIG. III-1. A view of the test flume looking upstream can be seen in PLATE III-2.

The supply discharge was recorded on a Foxboro chart recorder that was connected to pressure taps located on either side of the orifice fitting shown in FIG. III-1. A simple point gauge located at the downstream end of the

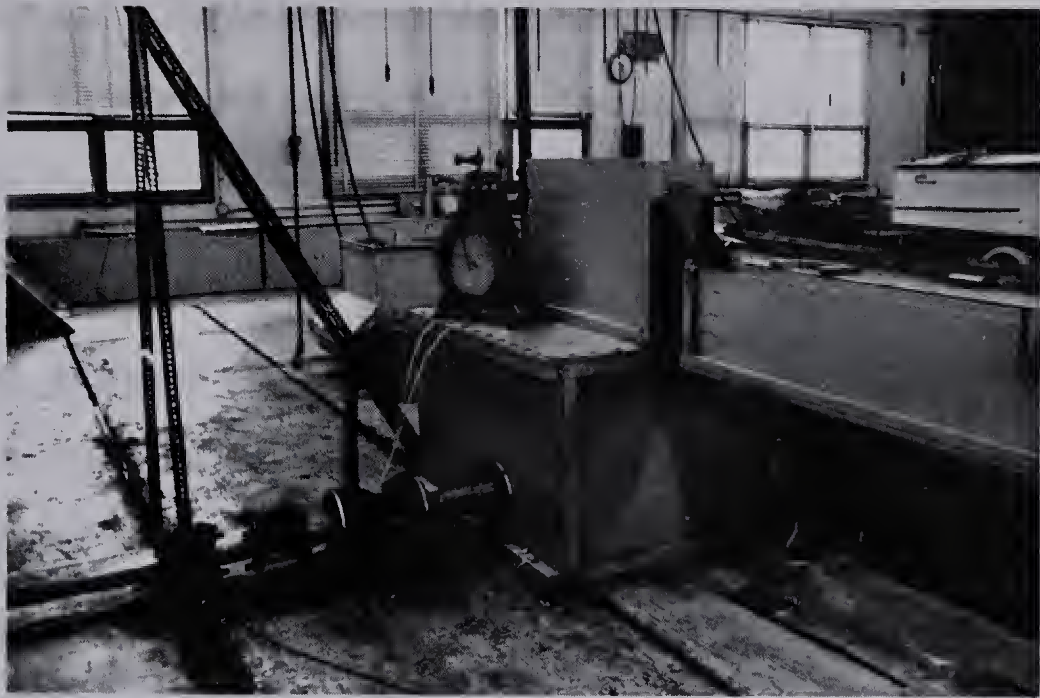

ENTRANCE TANK AND FLOW CONTROL VALVES

PLATE III-1

EXPERIMENTAL FLUME

PLATE III-2

flume, where open water conditions existed, was used to measure the initial undisturbed depth in the flume. Prior to testing, the flume was carefully leveled to ensure that the still water depth would be uniform over the entire length of the flume.

3.3 Surge Recording System

The surge recording system was designed to obtain a continuous record of surface elevation against time as a surge passed by each of several stations along the flume. The record at each station was referred to the same time origin, so that the time required for the toe of a surge to travel between stations could be determined. By plotting this time against distance along the flume and assuming a linear relationship, the average time for each of the recording stations was obtained by extrapolating or interpolating. The velocity of propagation of the toe of the surge could then be calculated for each recording station by the method outlined in APPENDIX "A". The system was originally designed to obtain records for five stations located at 25 ft. intervals along the flume, however, electrical interference in the recording system affected the accuracy of the data and therefore, restricted the maximum number of recording stations to three.

The surge recording system made use of a number of capacitive pressure transducers coupled to an X-Y recorder as illustrated in FIG. III-2. This system was

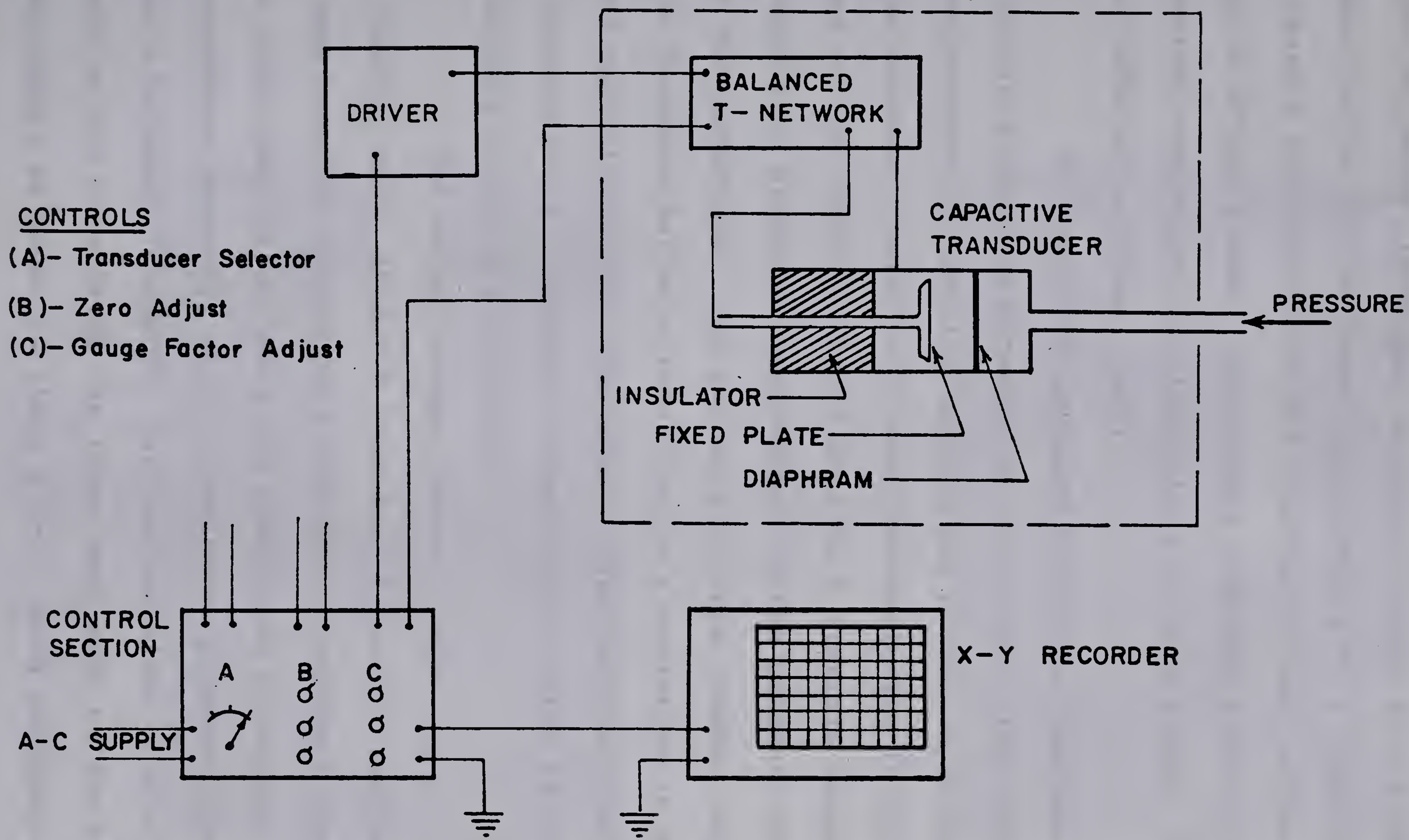

SCHEMATIC DIAGRAM PRESSURE TRANSDUCER SYSTEM

FIGURE III-2

designed and constructed at the University of Alberta. The following discussion has been limited to a brief description of the operating principle of a capacitive pressure transducer and the function of each of the component parts of the system. For a more complete discussion on the design, operation and limitations of this system, the reader is referred to Shook (1966).

A capacitive pressure transducer operates on the principle that the capacity of a parallel plate capacitor varies when the spacing between the plates is varied. In the pressure transducer, shown schematically in FIG. III-2, one of the parallel plates acts as a flexible diaphram subject to pressure fluctuations in the pressure chamber of the transducer. As pressure in this chamber varies, the diaphram deflects resulting in a variation in spacing and capacity of the transducer. This varying capacity is interpreted as a varying voltage signal which is then recorded on the X-Y recorder.

The actual system, shown in FIG. III-2, contains a Moseley Model 2A-2, X-Y recorder, a control section and three pressure transducers with each transducer requiring an individual driver unit and a balanced T-network. A transducer assembly, which contained a pressure transducer and a balanced T-network, was mounted along with a driver unit on the outside of the flume near each of the pressure tap points as shown in PLATE III-3. Each transducer pressure

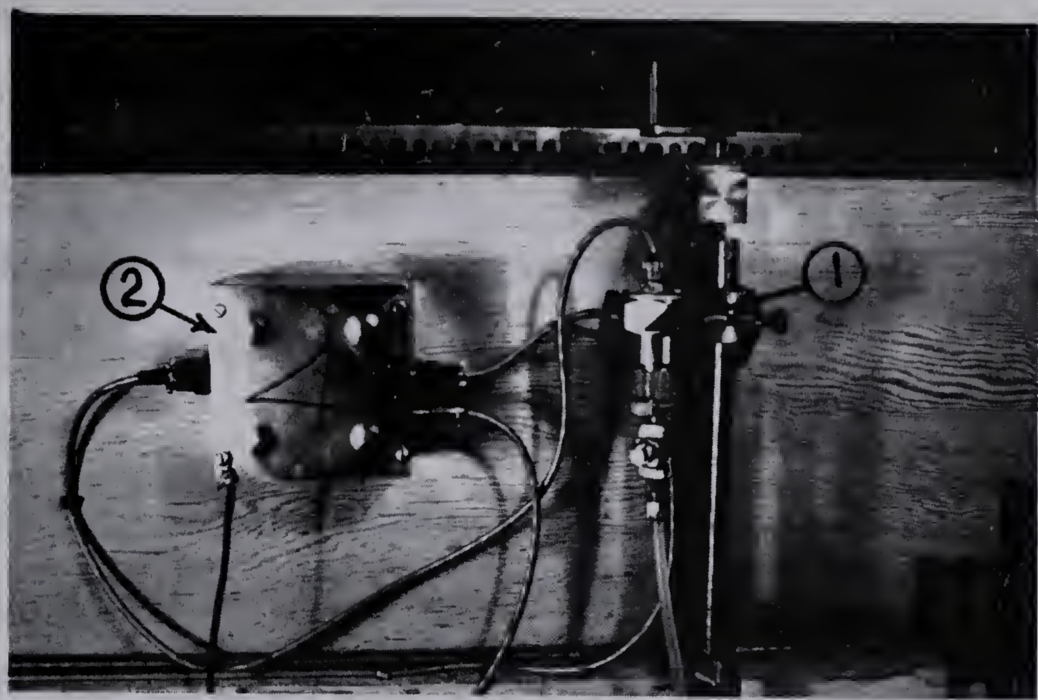

[1] PRESSURE TRANSDUCER ASSEMBLY
[2] DRIVER UNIT

PLATE III-3

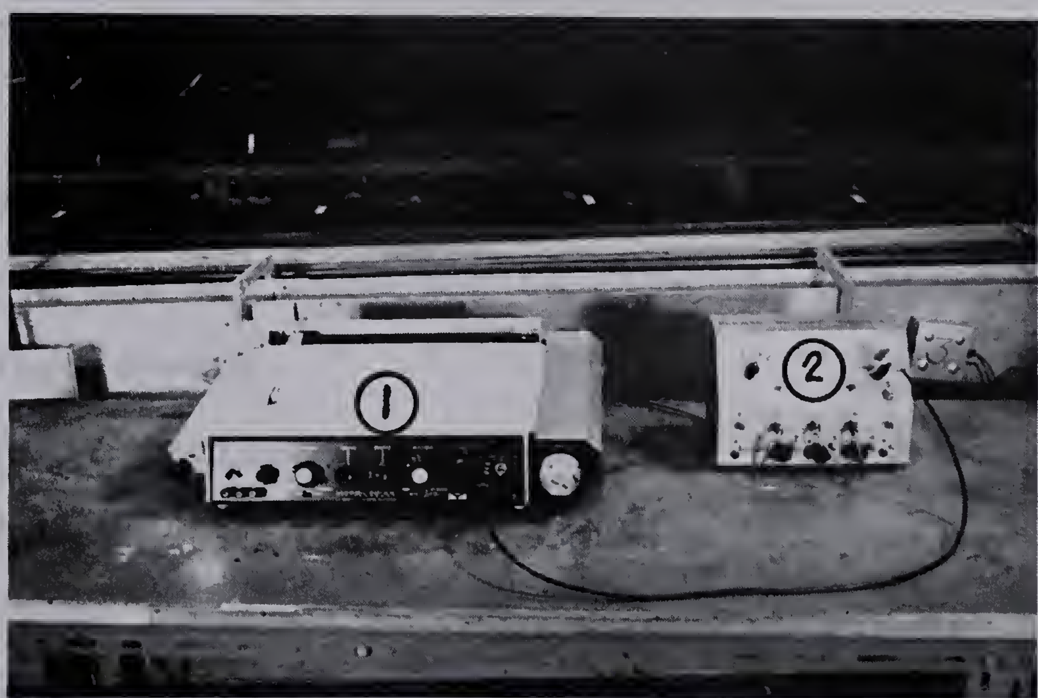

[1] X-Y RECORDER
[2] CONTROL SECTION

PLATE III-4

chamber was connected to the pressure tap hole in the bottom of the flume using ¼ in. plastic tubing. In order to minimize the length of the electrical leads and therefore the possibility of electrical interference, the X-Y recorder and control unit were located opposite the centre transducer. A view of the recorder and the control section can be seen in PLATE III-4.

The control section contained a main selector switch along with zero and gauge factor adjust controls for each of the transducers; it also served as a DC power supply for each of the driver units. The function of the main selector switch was to select the desired transducer signal for input to the recorder. For a given transducer pressure, the level of the transducer signal and therefore the position of the recording pen could be varied by the zero adjust controls. The gauge factor controls were used to calibrate the system; they vary the ratio between a given change in transducer pressure and the resulting deflection on the X-Y recorder to give the desired scale ratio or gauge factor.

The function of a driver unit is to convert the DC supply from the control section to an A-C square-wave voltage that is supplied to the balanced T-network.

Each balanced T-network contains a capacitor whose capacity is compared with the capacity of the corresponding transducer. If these capacities differ, a

voltage proportional to the difference is fed to the control section where it can be channeled through the selector switch to the recorder.

In practice a number of mechanical and electrical problems were encountered that affected the accuracy of the data; consequently, a sizeable portion of the time required for completion of the testing program was used in making refinements to the system.

3.4 Artificial Surface Covers

The most important aspect in the design of the test equipment was the selection of a material that would satisfactorily simulate a surface ice cover. This material was required to form a continuous surface cover having structural strength. Furthermore, the rigidity, surface roughness and weight of the cover were to be variable.

Michel (1965) advised the author that the only previous attempts to simulate a continuous ice sheet made use of paraffin or a mixture of paraffin, sawdust and coal. A search of the literature indicated that no other methods have been reported.

A number of pilot tests were conducted to determine if paraffin was suitable for simulating an ice cover. The results of these tests indicated that paraffin could only partially fulfil the above requirements. It was also evident from these tests that the operational problems

involved in using paraffin were sufficient cause for its rejection. These problems included the need for applying a new cover prior to each test and the difficulty in obtaining identical properties in subsequent covers.

The material finally selected to simulate a surface ice cover was ½ in. fir-plywood which was cut into strips 4-7/8 in. wide and 8 ft. long. These strips were connected, as shown in FIG. III-3 to form a continuous cover 104 ft. long. The cover was then placed in the flume leaving 16 ft. open at the downstream end, to allow for the measurement of undisturbed depth.

A total of five surface covers were used with rigidity, surface roughness and weight independently varied between covers. PLATES III-5 through III-8 show views of the covers used with the exception of Cover 4, which had identical properties to Cover 3 except a uniform load of 0.162 lb./ft. was added by placing 0.1 lb. steel washers on the top of the cover at a spacing of 0.6 ft. TABLE III-1 lists, in tabular form, the relative properties of each of the covers and indicates the method that was used to obtain these properties. Stiffness was reduced by making a series of transverse cuts, 3/8 in. deep, on both sides of the cover. The cuts were spaced at 2 in. and staggered on opposite sides. Surface roughness was varied by affixing materials of varying roughness to the surface in contact with the water and weight was varied by the addition of

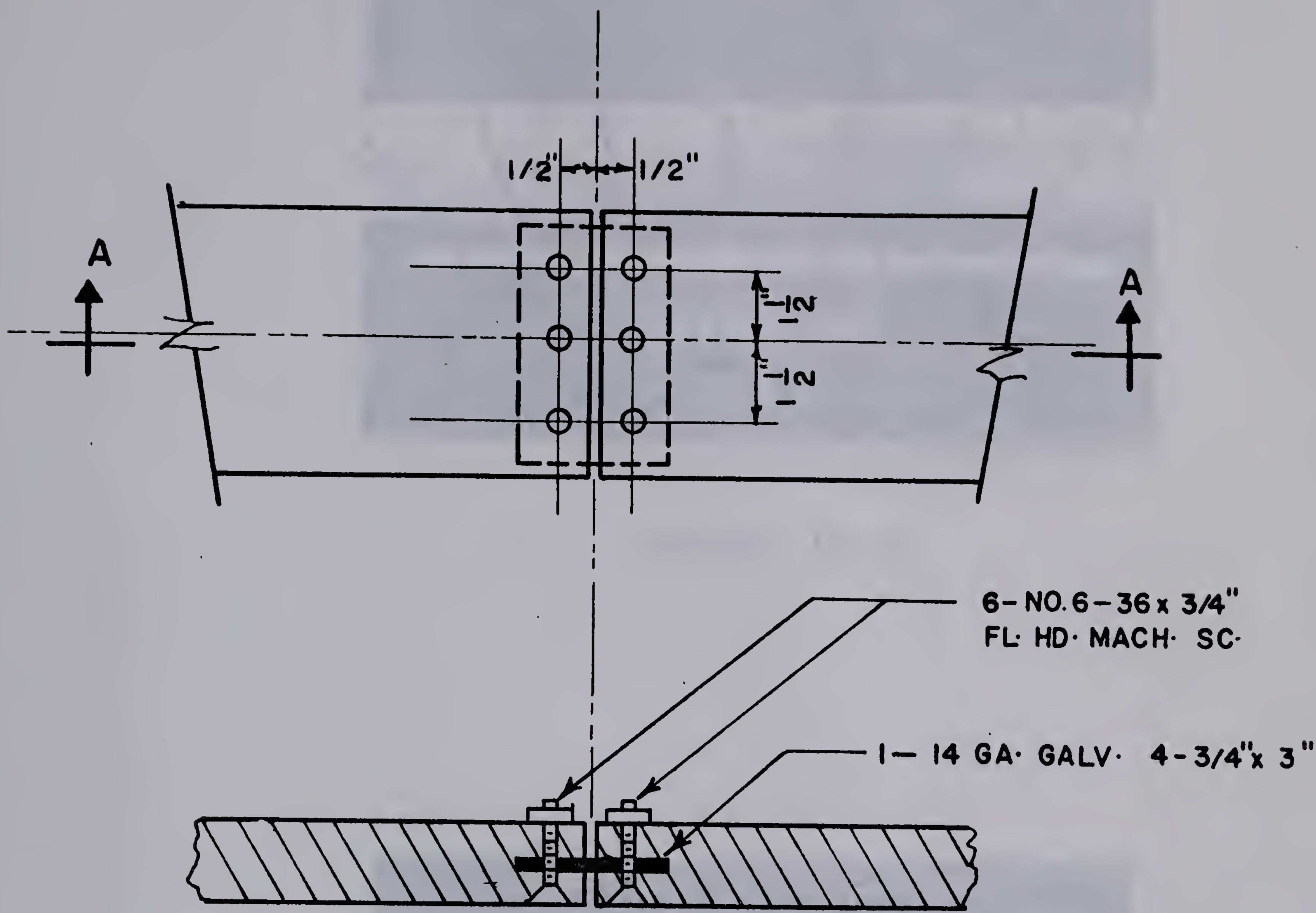

SECTION A-A

TYPICAL COVER CONNECTION

FIGURE III-3

PLATE III–5

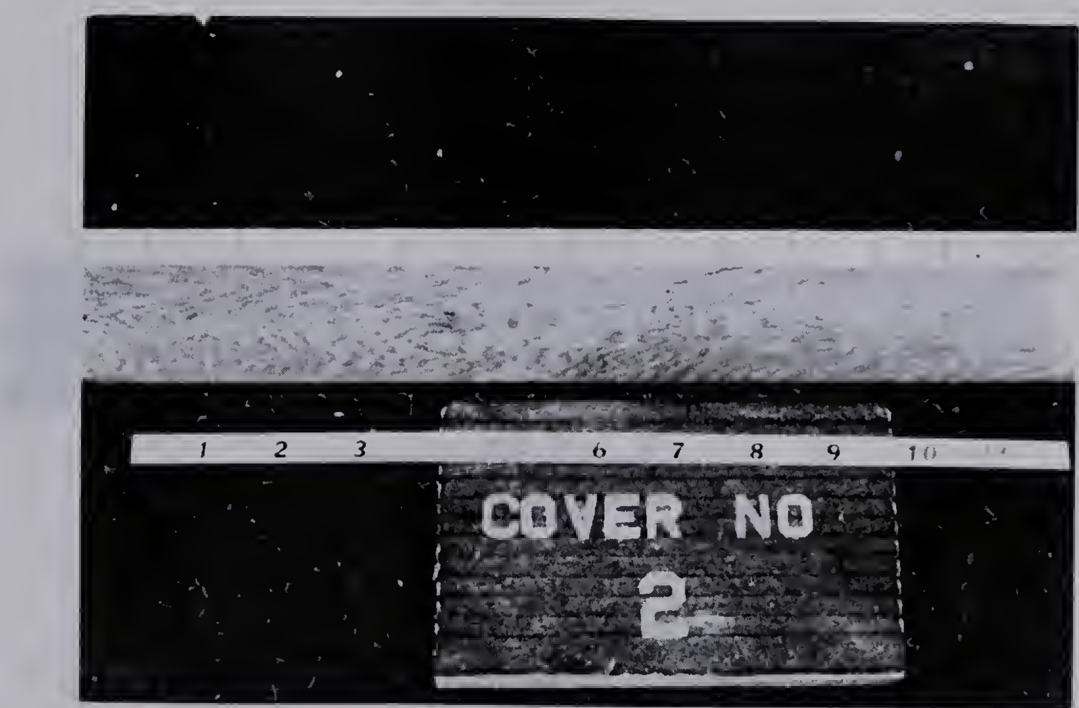

PLATE III–6

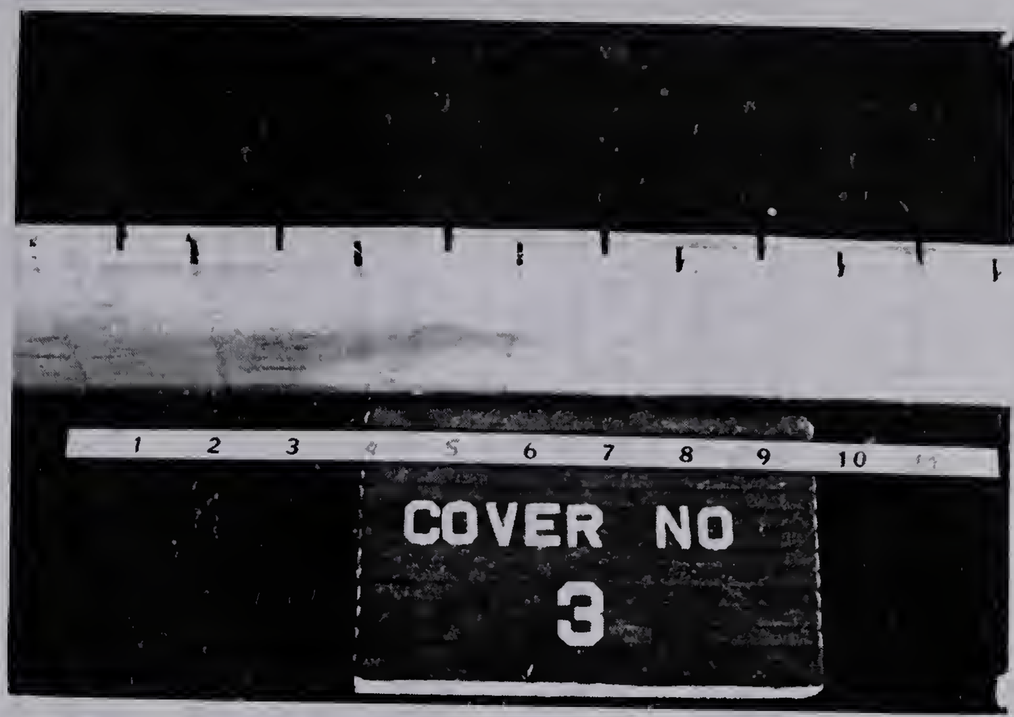

PLATE III-7

PLATE III-8

TABLE: III - 1

SURFACE COVER PROPERTIES

COVER NUMBER	SUBMERGED THICKNESS h_s (ft.)[1]	RELATIVE RIGIDITY	RELATIVE ROUGHNESS	REMARKS
1	0.031	flexible	fairly smooth	-Transverse cuts made 3/8 in. deep, spaced at 2 in., staggered on either side -Unfinished surface
2	0.031	stiff	smooth	-No transverse cuts -Unfinished surface
3	0.031	flexible	smooth	-Polyethylene sheet affixed to one surface of Cover 1.
4	0.039	flexible	smooth	-Surcharge of 0.162 lb./ft. added to the top of Cover 3 by placing 0.1 lb. steel washers at 0.6 ft.
5	0.044	flexible	rough	-Rough rubber floor matting affixed to one surface of Cover 3.

[1]Covers 1 through 4 had an average thickness of 0.50 in., Cover 5 had a maximum thickness of 0.635 in., and a minimum thickness of 0.58 in.

a uniform surcharge to the upper surface of the cover.

3.5 Calibration of The Recording System

The pressure transducer system was calibrated daily, prior to testing, to give a gauge factor of unity for each of the transducers. The calibration procedure entailed setting each gauge factor adjust control so that a 5 in. increment in head over a transducer would result in a corresponding 5 in. deflection of the recorder pen. This increment, which was several times larger than the actual surge heights measured, was chosen to minimize the percentage error in calibration while remaining in the range where transducer response was linear for all practical purposes.

Upon completion of testing, a final value of gauge factor was determined for each transducer. This value was assumed to be correct for all the tests run that day and was therefore used as a correction coefficient on the surge height values taken from the recorder charts.

3.6 Experimental Procedure

Before each test, with the butterfly valve open, the plug valve was set to give a desired supply discharge. The butterfly valve was then closed, shutting off flow to the flume and the level of water in the flume was set at a predetermined value. Undisturbed piezometric depth was observed after allowing an interval of about fifteen minutes

for the water in the flume to come to rest. The supply flow was then rapidly turned on causing a surge to form at the head of the flume. As the surge travelled through the flume, the pressure transducer system was operated so that the surge profile was recorded as the surge passed by each of the recording stations along the flume. FIG. III-4 shows a number of typical surge records.

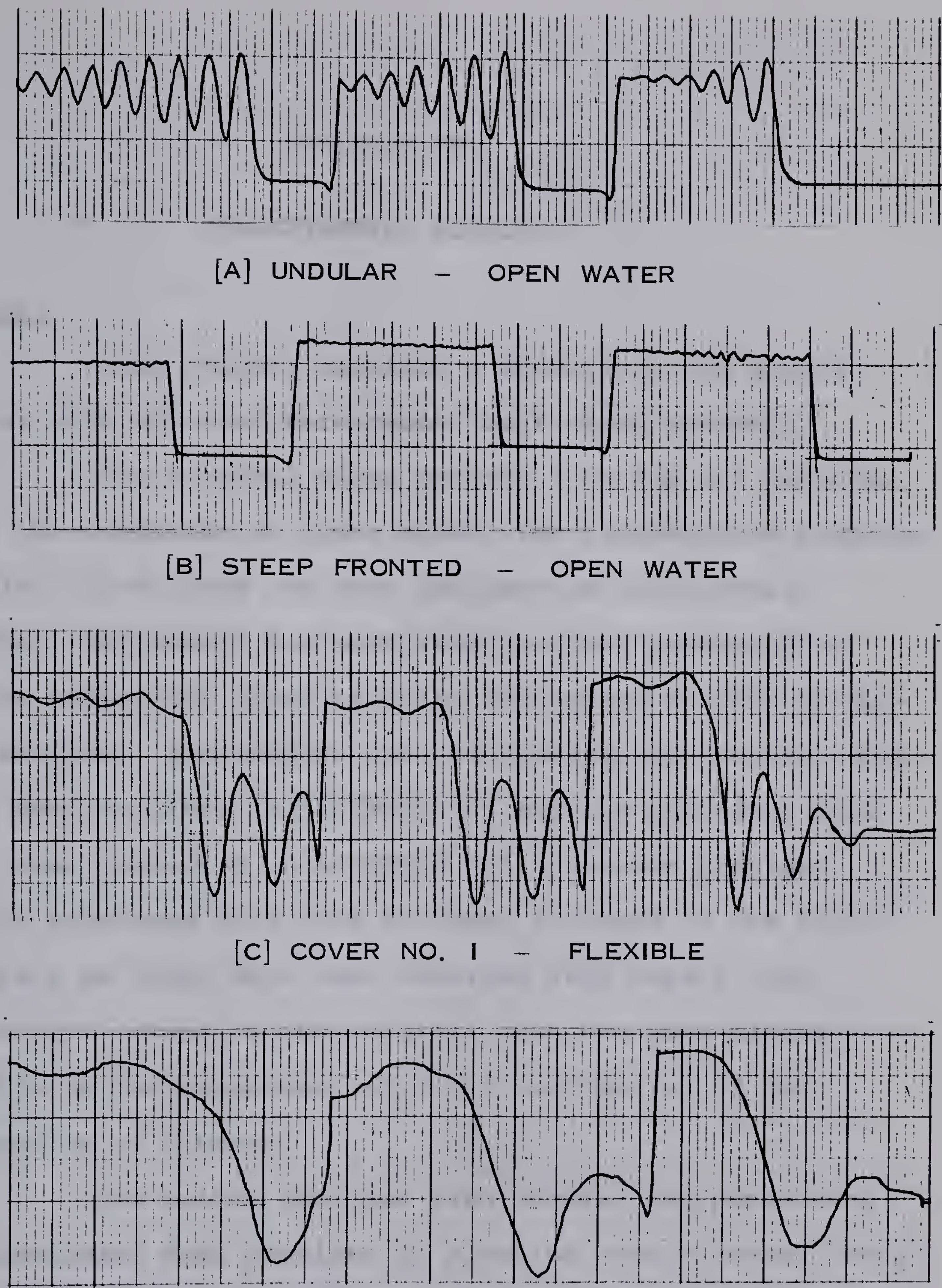

[A] UNDULAR – OPEN WATER

[B] STEEP FRONTED – OPEN WATER

[C] COVER NO. 1 – FLEXIBLE

[D] COVER NO. 2 – STIFF

TYPICAL SURGE RECORDS

FIGURE III-4

CHAPTER IV

EXPERIMENTAL RESULTS

4.1 General

This chapter contains a summary of the experimental data obtained throughout the testing program.

The original surge records from the X-Y recorder, with the exception of those shown, for illustrative purposes, in FIG. III-4, have not been included in this report, however, the record for each test has been processed to obtain values for surge velocity and height at each measuring station. The methods used to process the original data have been outlined in APPENDIX "A" and the processed data have been tabulated in APPENDIX "B". Certain portions of the processed data have not been included in the final analysis as these data were obtained from repeat runs. The entire volume of the original data has been placed on file in the Department of Civil Engineering of the University of Alberta.

The method that has been adopted for presenting the processed data consists of plotting Froude number based on surge velocity $V_w/\sqrt{gy_o}$ against non-dimensional surge height η/y_o. It was selected because of the relationship known to exist between these two parameters for open water

surges. In using this approach, it was hoped that the effect of each of the variables imposed by the addition of a surface cover, on the relationship between $V_w/\sqrt{gy_o}$ and η/y_o could be assessed.

A number of surface profiles have been plotted for both open water and surface cover conditions to demonstrate the effect that a surface cover has on surge profiles.

The experimental data have been classified for the cover condition under which the tests were conducted and subclassified for the approximate undisturbed piezometric depth that was used for a particular series of tests. TABLE IV-1 shows the range of conditions for which the results contained in this chapter were obtained.

4.2 Surge Height-Velocity Relationship for Open Water Conditions

The processed data for open water surges have been plotted arithmetically in FIG. IV-1, as Froude number based on surge velocity $V_w/\sqrt{gy_o}$ against maximum non-dimensional surge height $\eta max/y_o$. The dashed line shown in the left of this figure has been taken from the undular surge results obtained by Sandover and Zienkiewicz (1957). These data have also been plotted in FIG. IV-2 as Froude number $V_w/\sqrt{gy_o}$ against average non-dimensional surge height $\eta ave/y_o$. The form of the surface profile and the

TABLE: IV - 1

INDEX OF PROCESSED DATA

SERIES	UNDISTURBED PIEZOMETRIC DEPTH y_p (ft.)	SURFACE CONDITION
021 - 025 031 - 035 041 - 045	0.2 0.3 0.4	Free Surface
1021-1024 1231-1234* 1041-1044	0.2 0.3 0.4	Cover Number 1 - Flexible - Smooth
2121-2125* 2331-2338* 2141-2148	0.2 0.3 0.4	Cover Number 2 - Stiff - Smooth
3021-3027 3031-3037 3041-3038	0.2 0.3 0.4	Cover Number 3 - Flexible - Very Smooth
4021-4027 4021-4038 4041-4047	0.2 0.3 0.4	Cover Number 4 - Cover #3 with a surcharge of 0.162#/ft.
5021-5025 5031-5035 5041-5045	0.2 0.3 0.4	Cover Number 5 - Flexible - Very Rough

*Repeat runs made under these conditions.

Notes:

1. Undisturbed depth is the approximate piezometric level in the flume and is subject to correction for surface cover data.

2. Discharge range was 0 to 0.5 cfs. for each series.

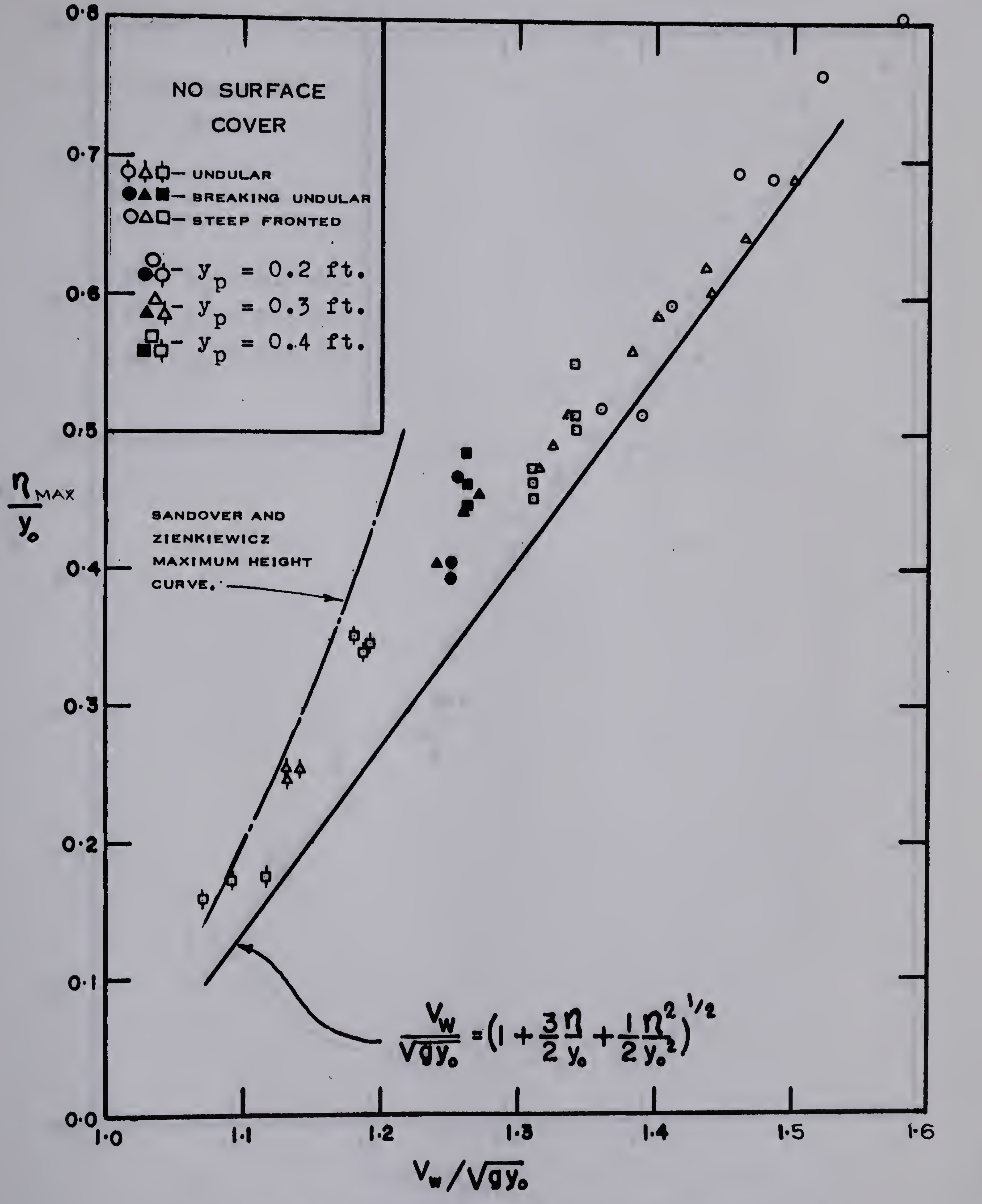

MAXIMUM SURGE HEIGHT – VELOCITY RELATIONSHIP

FIGURE IV–I

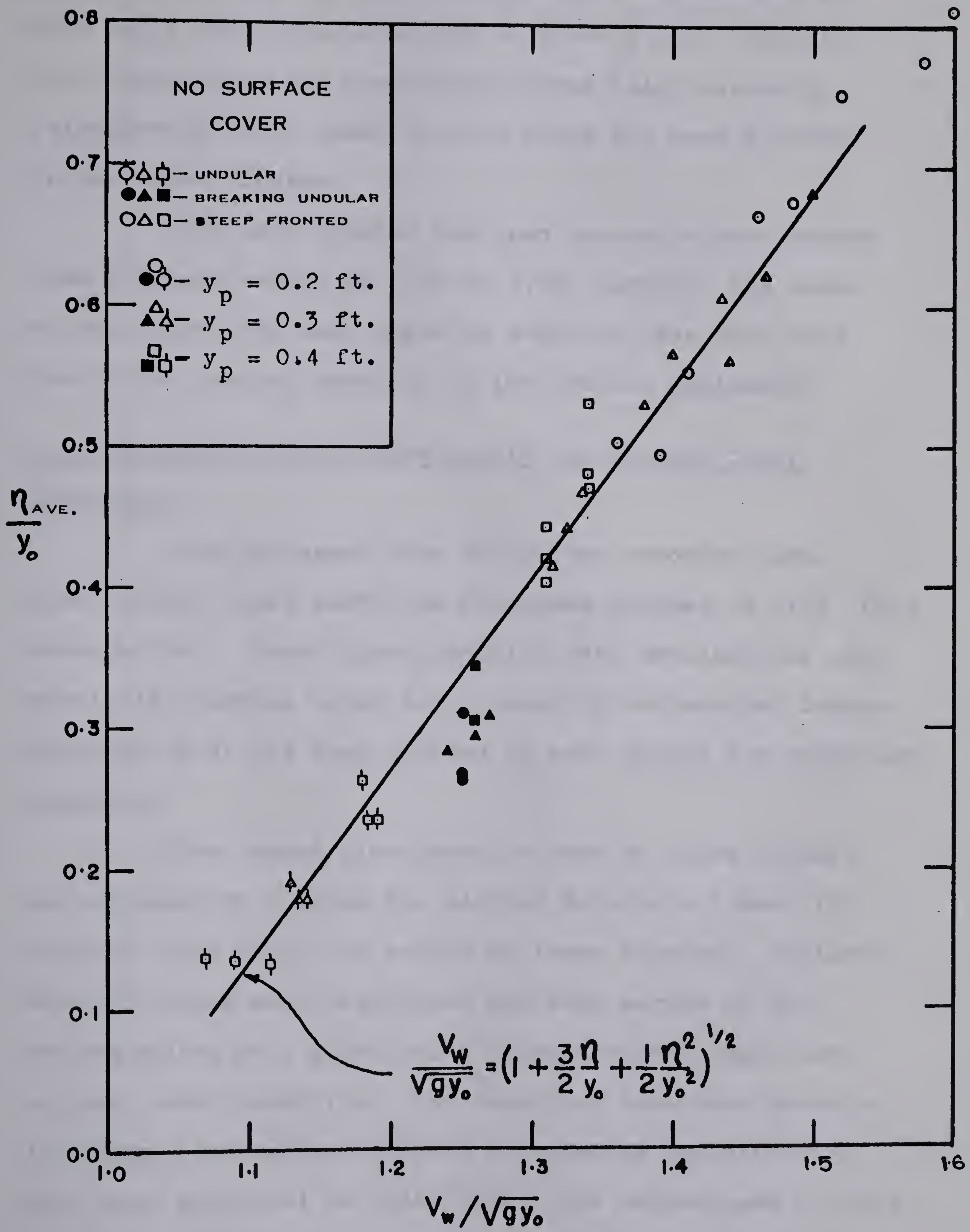

AVERAGE SURGE HEIGHT – VELOCITY RELATIONSHIP

FIGURE IV–2

approximate value of undisturbed depth corresponding to each point have been indicated in these plots. Equation (2-3) describing the theoretical surge height-velocity relationship for a steep fronted surge has been plotted in the above figures.

The data plotted for open channel surges ranges from a Froude number of 1.07 to 1.58, however, the range of data shown for each depth is somewhat less than this due to the limited capacity of the testing equipment.

4.3 Surge Height-Velocity Relationship for Surface Cover Conditions

The processed data for surges recorded under each surface cover condition have been plotted in FIGs. IV-3 through IV-7. Each figure contains data obtained for one particular surface cover and a range of undisturbed depths. Equation (2-3) has been plotted in each figure for reference purposes.

The dashed line shown in each of these figures was obtained by fitting the plotted data with a best fit straight line using the method of least squares. Similarly, best fit lines were calculated for each series of data corresponding to a given value of undisturbed depth and a given cover condition. The resulting equations describing these lines along with the correlation coefficients have been tabulated in TABLE IV-2. The method used in this

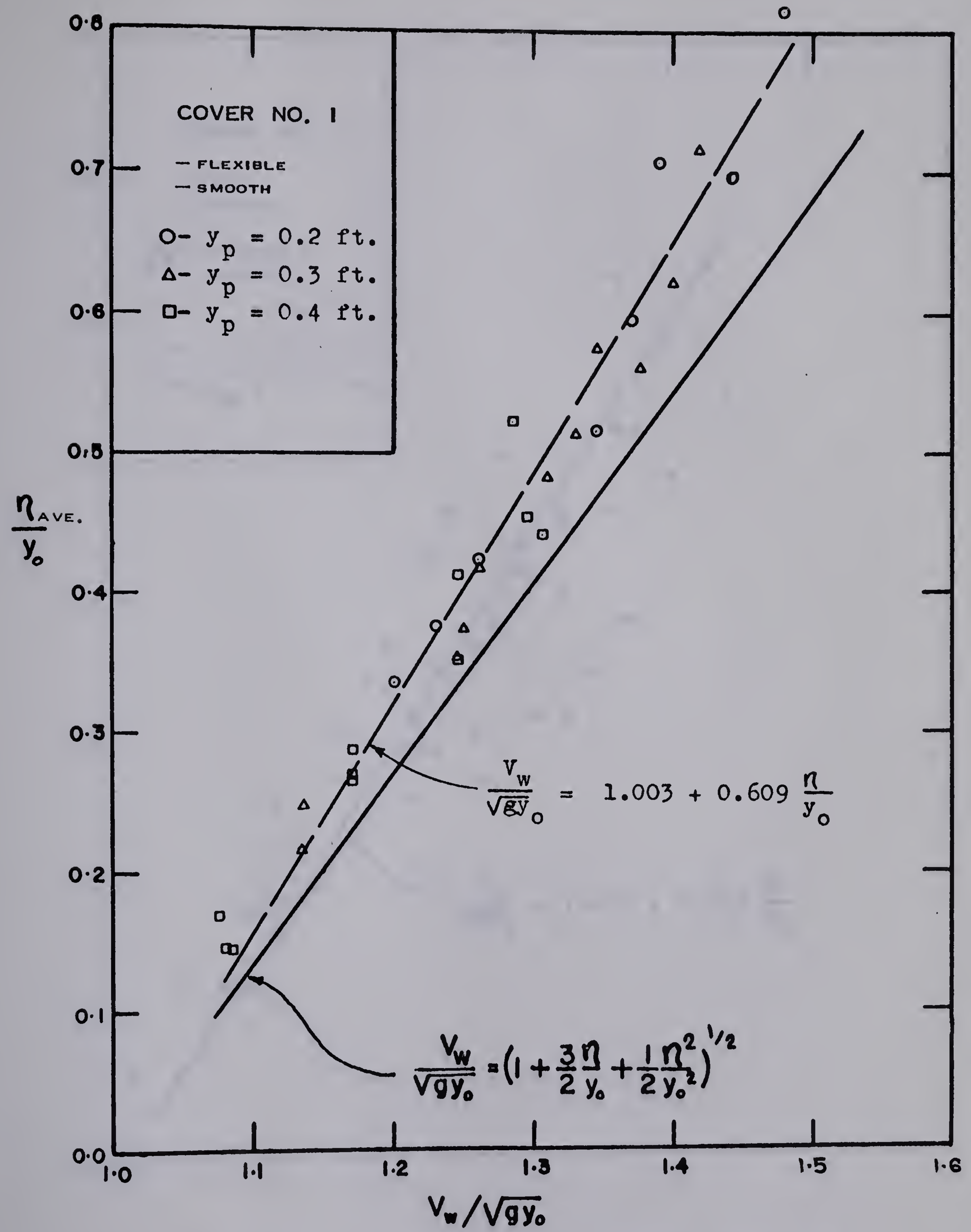

AVERAGE SURGE HEIGHT – VELOCITY RELATIONSHIP

FIGURE IV–3

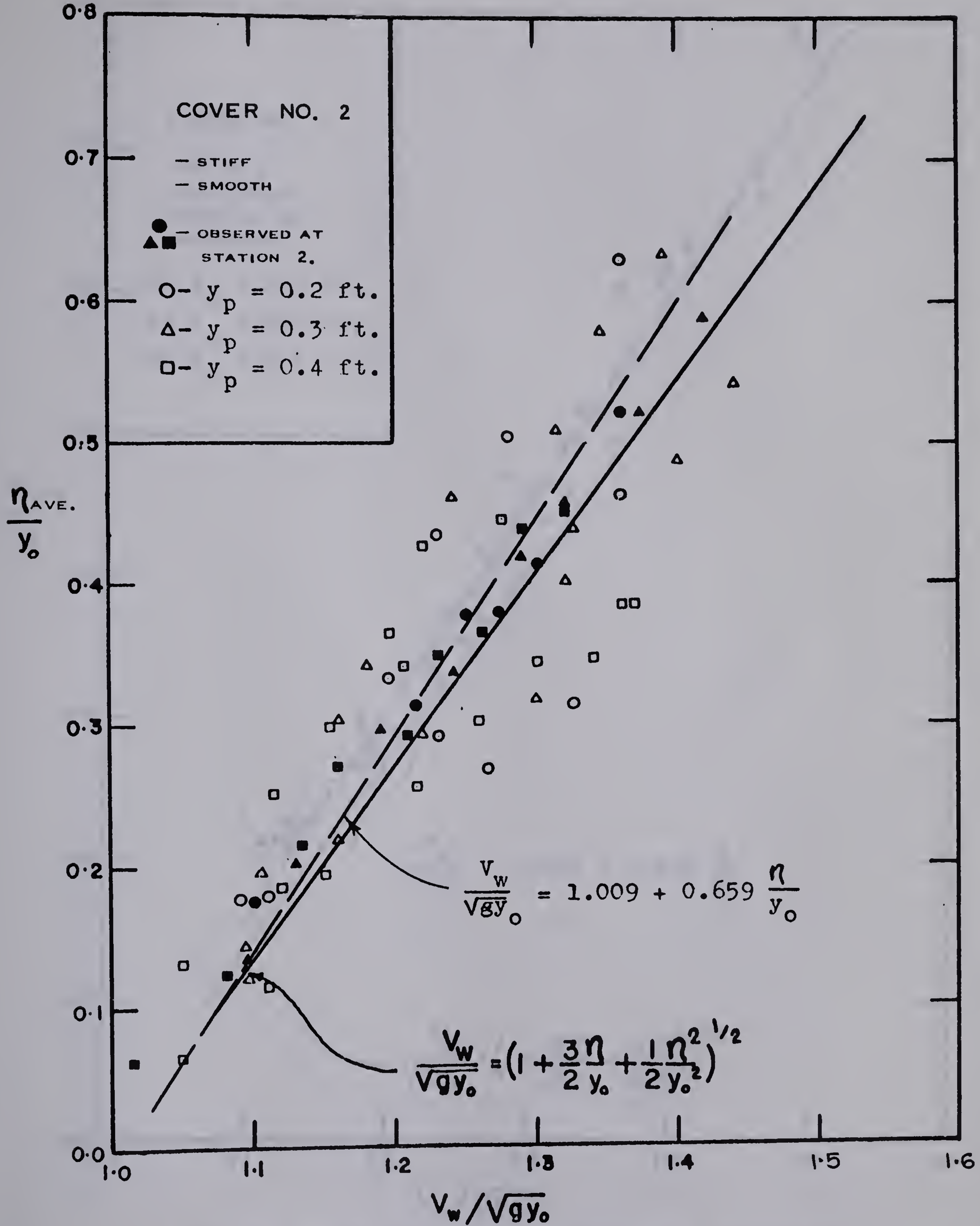

AVERAGE SURGE HEIGHT – VELOCITY RELATIONSHIP

FIGURE IV–4

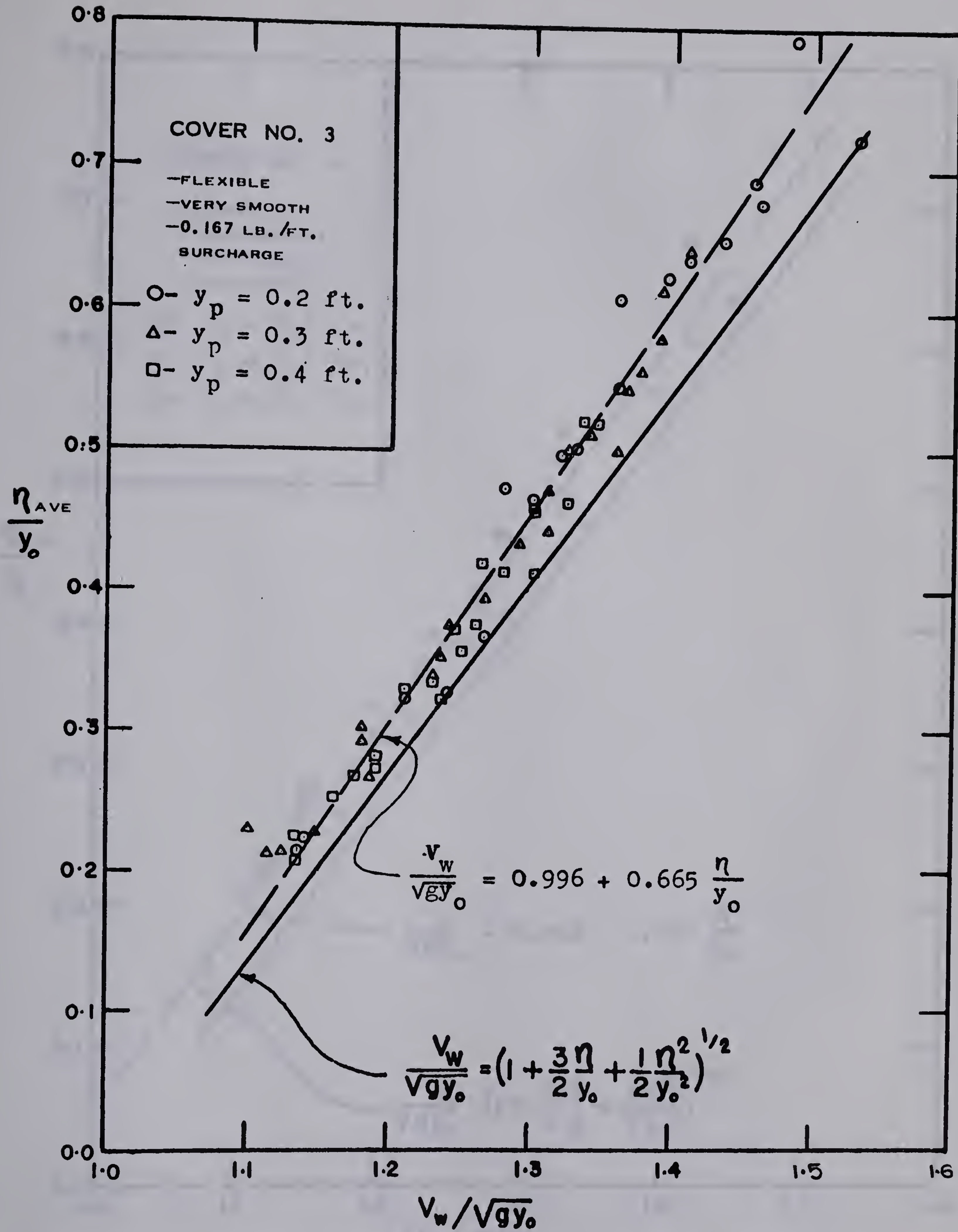

AVERAGE SURGE HEIGHT – VELOCITY RELATIONSHIP

FIGURE IV–5

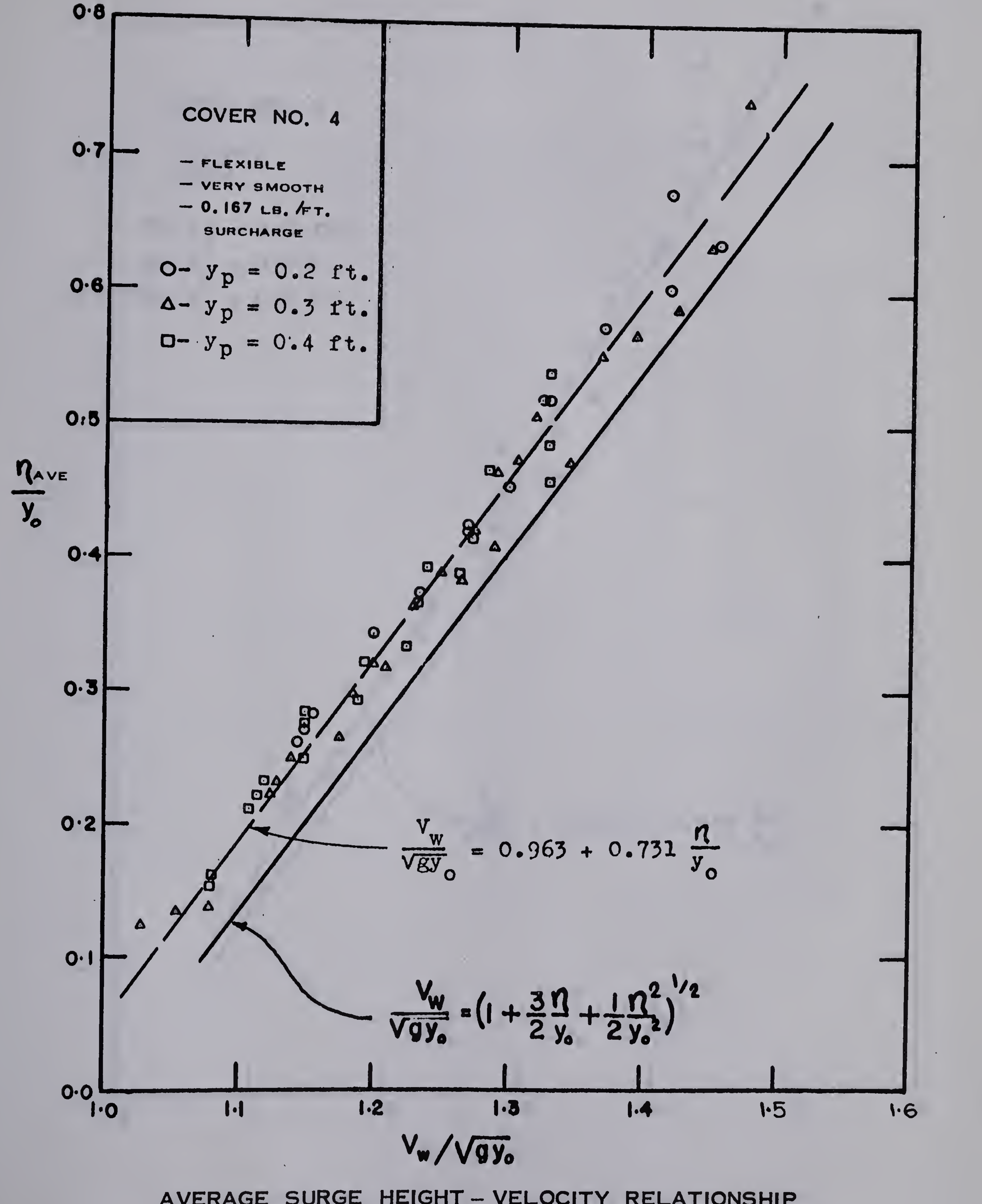

AVERAGE SURGE HEIGHT – VELOCITY RELATIONSHIP

FIGURE IV–6

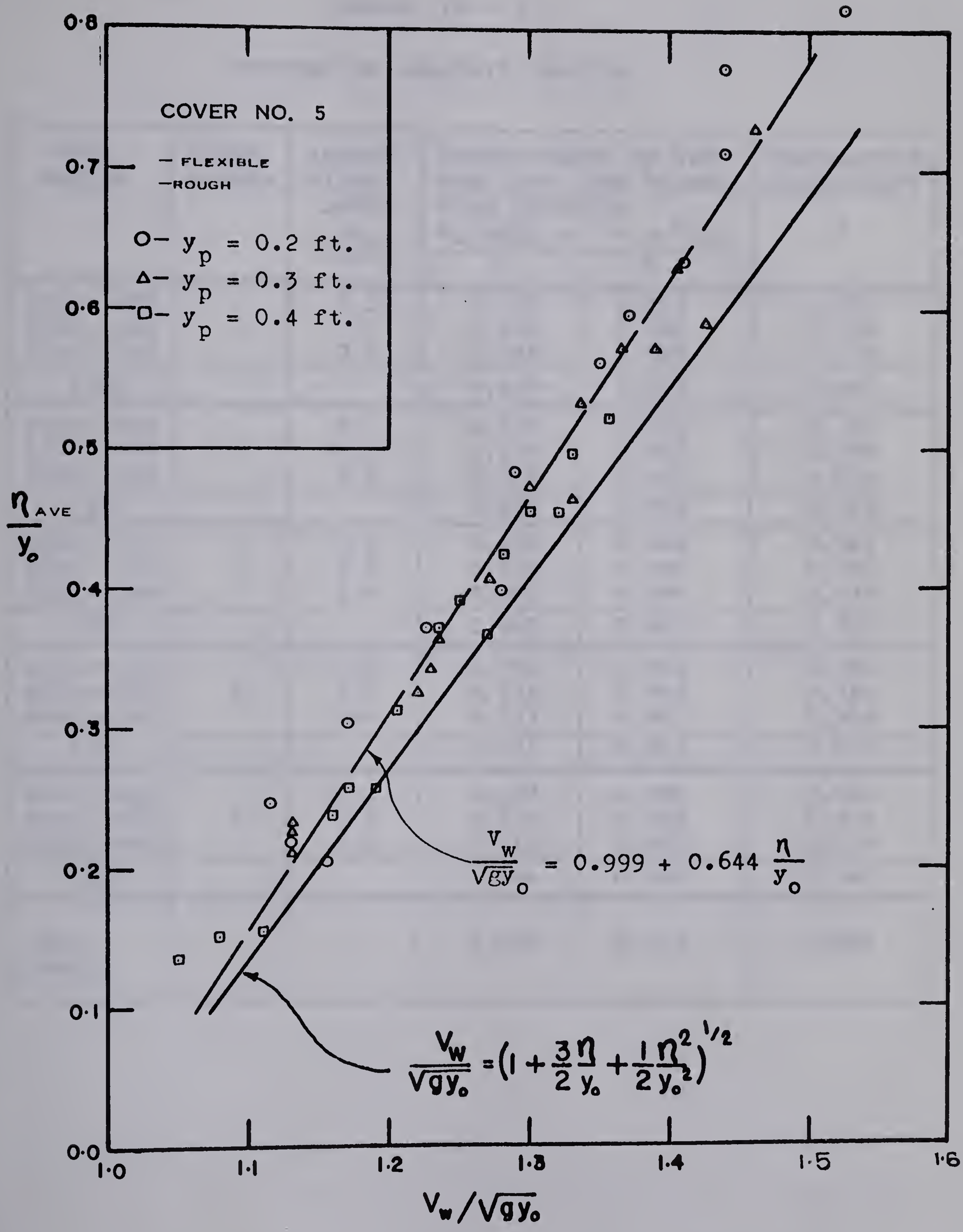

AVERAGE SURGE HEIGHT – VELOCITY RELATIONSHIP

FIGURE IV–7

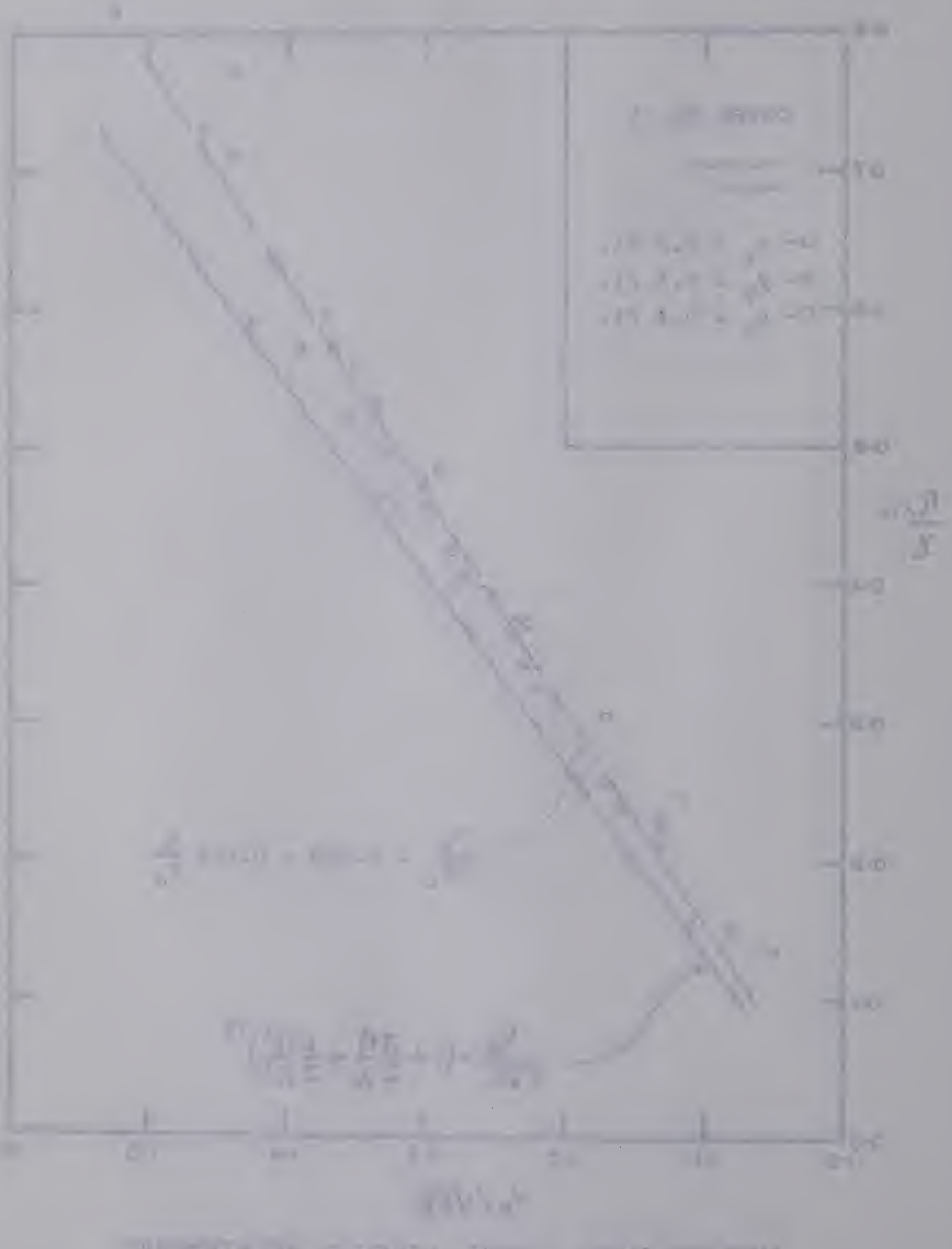

TABLE: IV - 2

REGRESSION ANALYSIS RESULTS

TEST SERIES	COVER NUMBER	APPROX. PIEZO. DEPTH y_p (ft.)	COEFFICIENTS OF THE STRAIGHT LINE REGRESSION EQUATION $V_w/\sqrt{gy_o} = b + a\,\eta/y_o$		CORRELATION COEFFICIENT r^2
			a	b	
1021-1024	1	0.2	0.572	1.022	0.957
1031-1034		0.3	0.618	1.006	0.974
1041-1044		0.4	0.645	0.992	0.928
1000			0.609	1.003	0.965
2121-2125	2	0.2	0.566	1.041	0.700
2331-2338		0.3	0.679	1.003	0.865
2141-2148		0.4	0.722	0.992	0.654
2000			0.659	1.009	0.768
3021-3027	3	0.2	0.661	0.994	0.941
3031-3037		0.3	0.696	0.987	0.977
3041-3048		0.4	0.683	0.994	0.939
3000			0.665	0.996	0.957
4021-4027	4	0.2	0.740	0.952	0.986
4031-4038		0.3	0.739	0.965	0.981
4041-4047		0.4	0.733	0.967	0.966
4000			0.731	0.963	0.981
5021-5025	5	0.2	0.623	0.996	0.969
5031-5035		0.3	0.678	0.988	0.974
5041-5045		0.4	0.715	0.982	0.970
5000			0.644	0.999	0.965
All Covers			0.659	0.997	0.894

analysis has been discussed in APPENDIX "A".

The data plotted in FIG. IV-4 for Cover 2 shows a considerable amount of scatter as indicated by a correlation coefficient of 0.768 for the linear relationship between $V_w/\sqrt{gy_o}$ and η/y_o. This can possibly be explained by noting that the portion of the data responsible for this poor correlation was obtained from the surge records at station 1 and station 3. This suggests that the assumption of a linear relationship between surge velocity and distance along the flume (see Sect. 3.3) is not valid for the tests conducted for Cover 2 which was considerably stiffer than the other covers used.

4.4 Surface Profiles

By assuming that the calculated surge velocity is correct for each point on the surface of a surge as it passes over a measuring station, the surface profile of that surge can be determined. This method (as outlined in APPENDIX "A") is at best approximate, as the profile obtained by measuring the change in depth at a fixed point does not give a true instantaneous surface profile due to a gradual variation in both profile and velocity with time. Also, the calculated velocities are for the toe of the surge and are not necessarily applicable to the undulations forming the overall surge profile. However, Sandover and Zienkiewicz (1957) have shown that surface profiles obtained

by this method for undular surges under open water conditions compare favorably with instantaneous surface profiles obtained photographically.

FIG. IV-8 demonstrates the three surface profile phases that were observed throughout the range of open water testing. The undular, undular-breaking and two steep fronted profiles plotted in this figure were obtained from the 031-035 Series for surges having Froude numbers of 1.13, 1.26, 1.32 and 1.46 respectively.

FIGs. IV-9 and IV-10 show the effect of the various surface covers on the surface profile of a surge. The profiles plotted in these figures have been obtained from surges having approximately equal values of Froude number and undisturbed piezometric depth, with each surge representing a different cover condition.

FIG. IV-11 contains a number of surface profiles obtained from the 3031 - 3037 Series of tests, for a range of Froude numbers. These plots are intended to demonstrate the changes in surface profile that occur under surface cover conditions as Froude number and non-dimensional surge height increase.

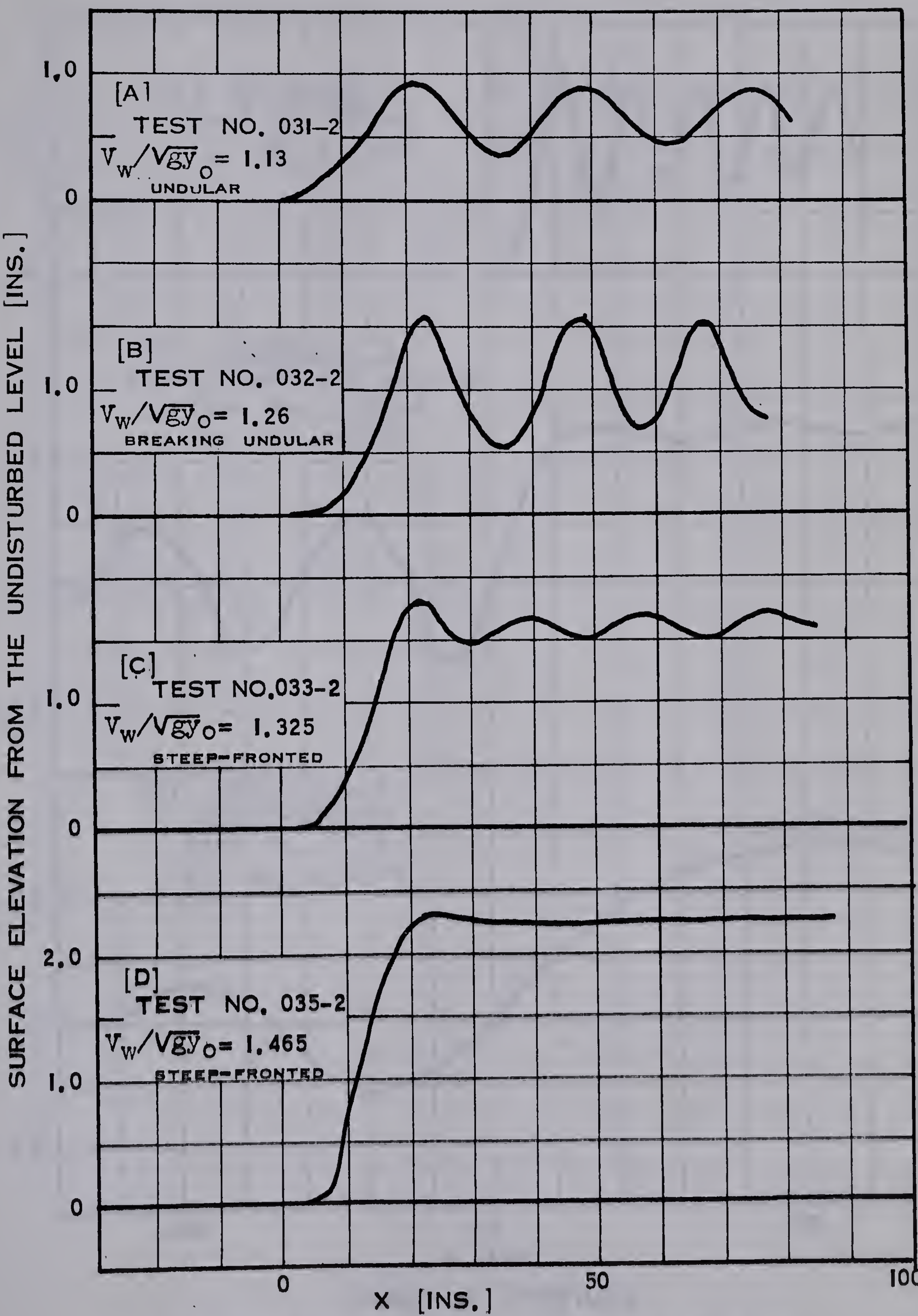

SURFACE PROFILES FOR OPEN WATER SURGES

FIGURE IV–8

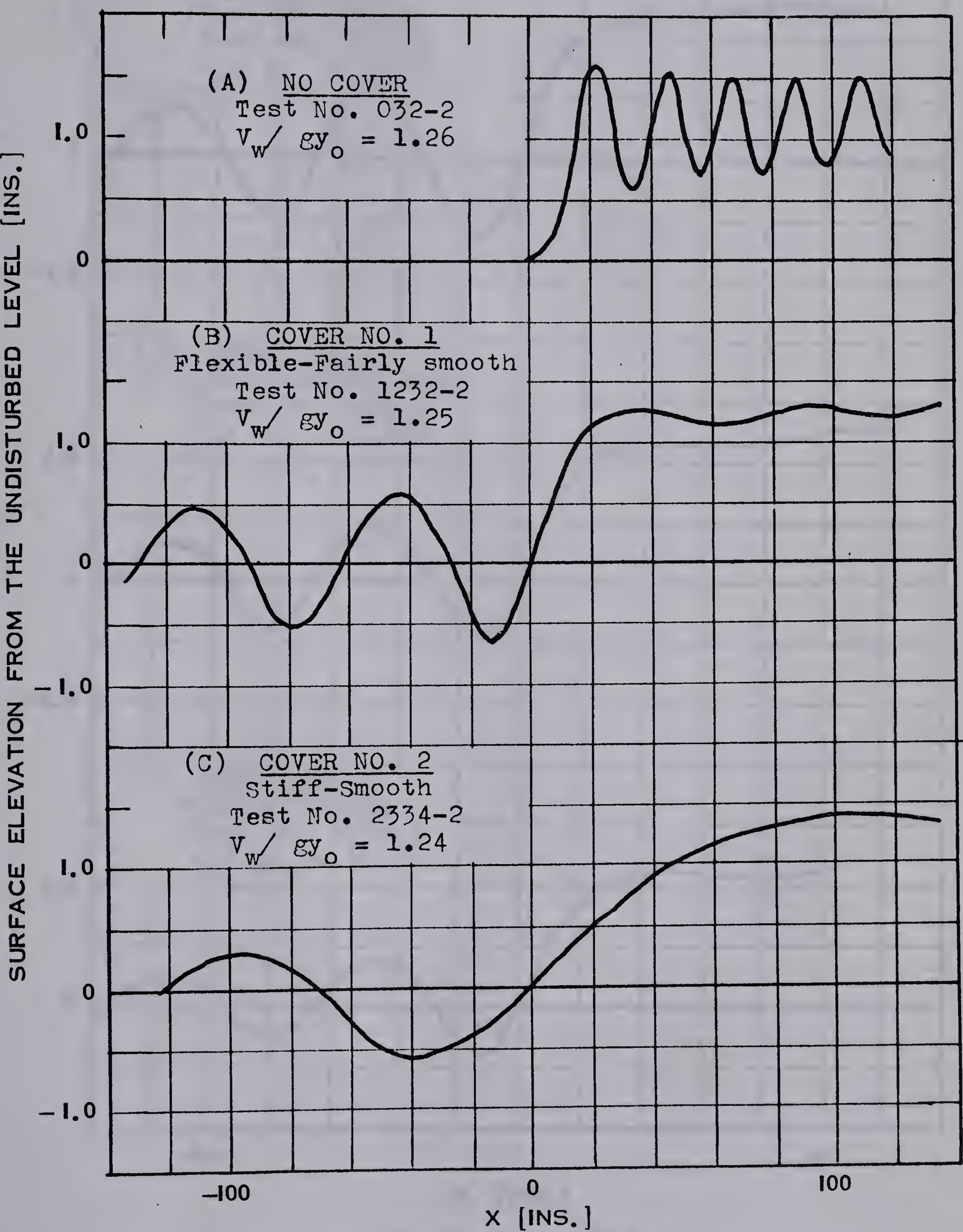

SURFACE PROFILES

FIGURE IV-9

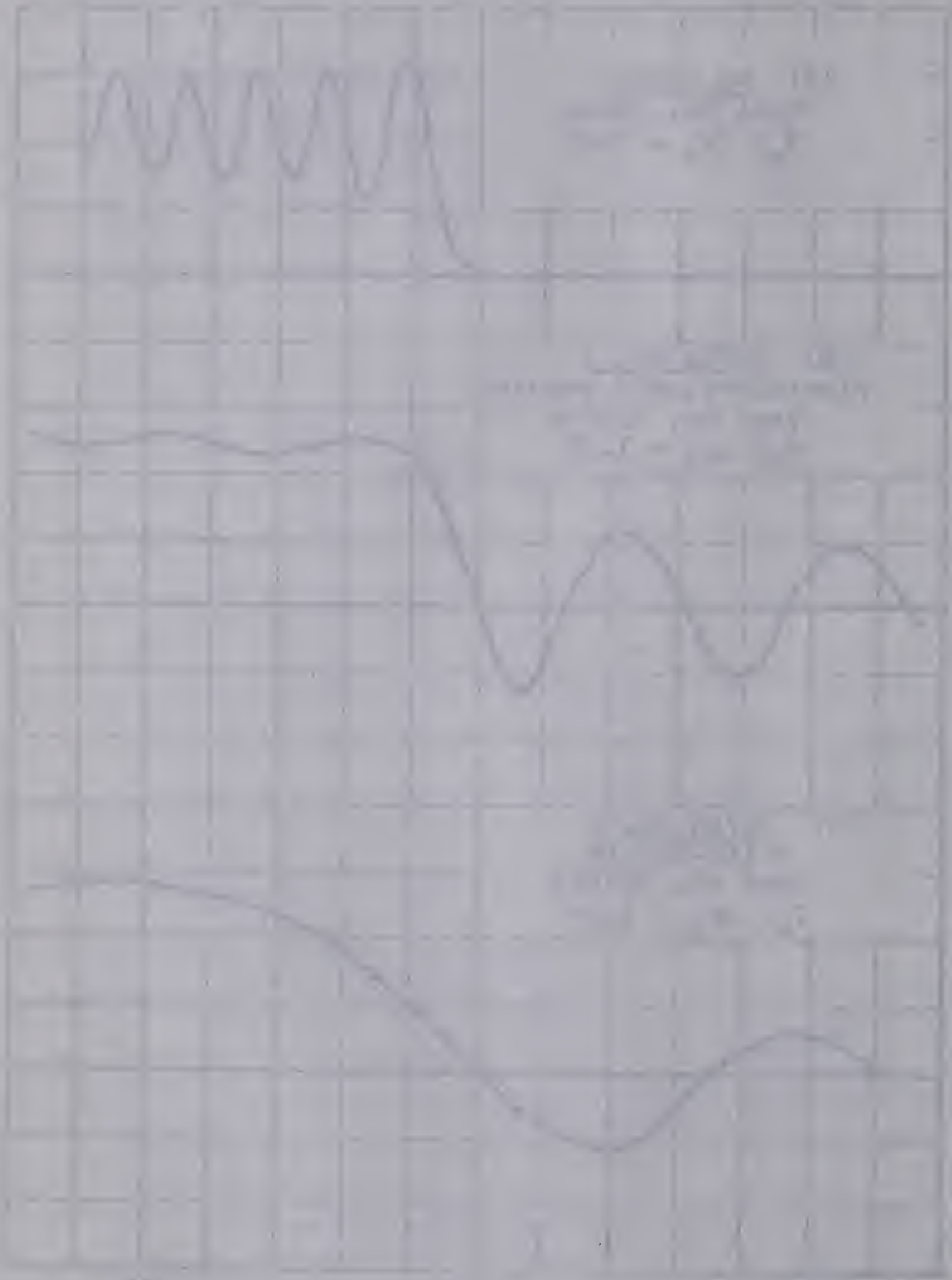

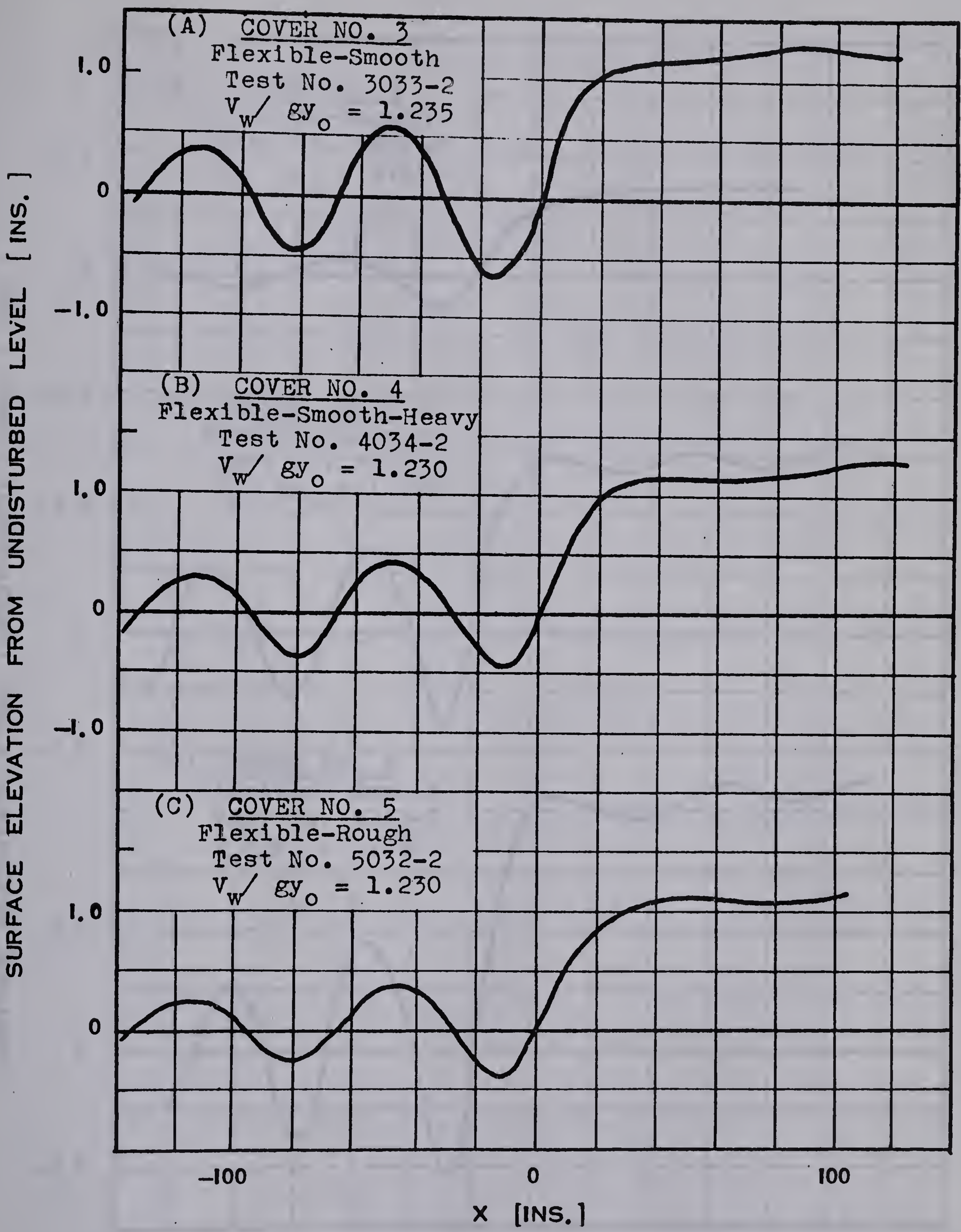

SURFACE PROFILES

FIGURE IV-10

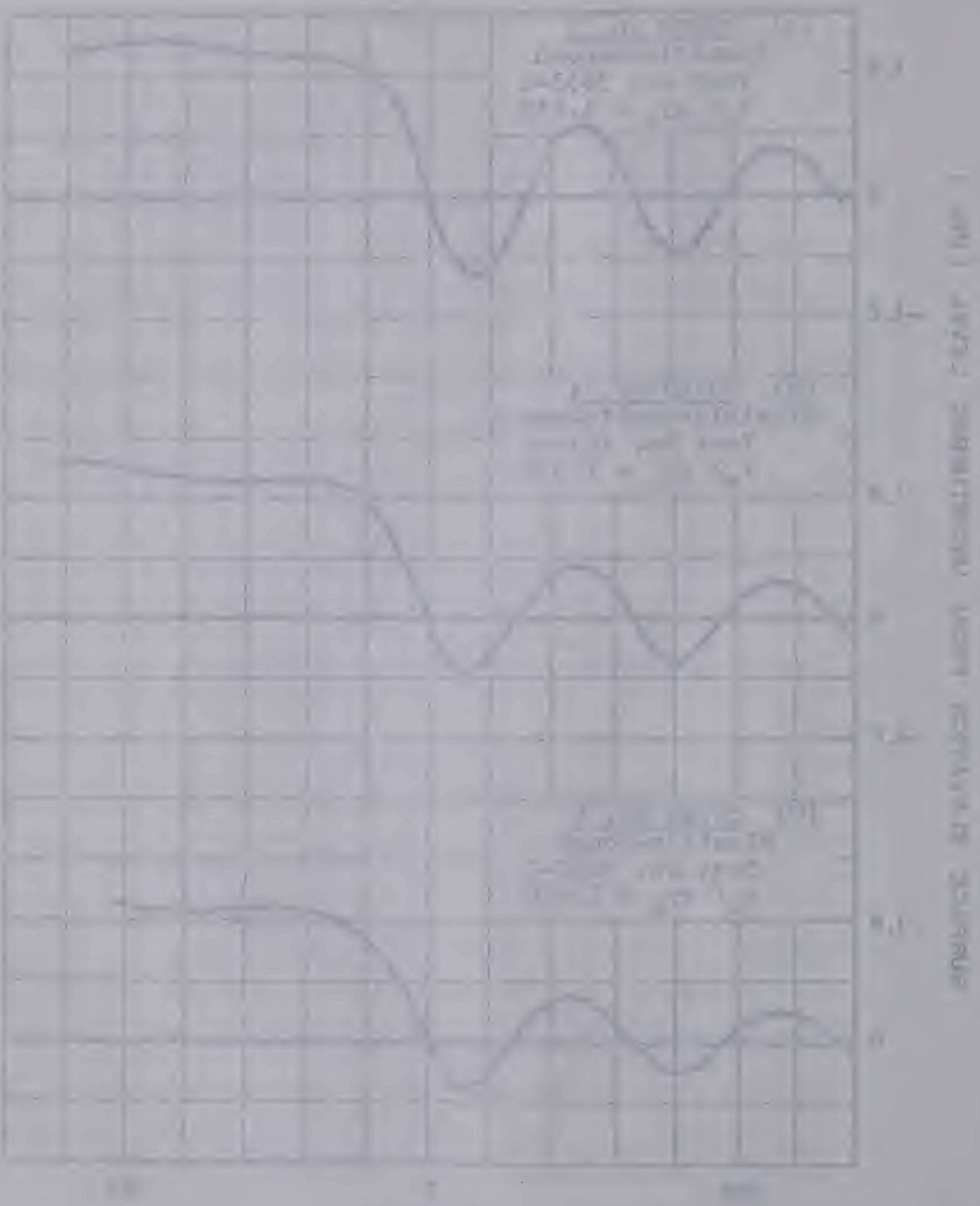

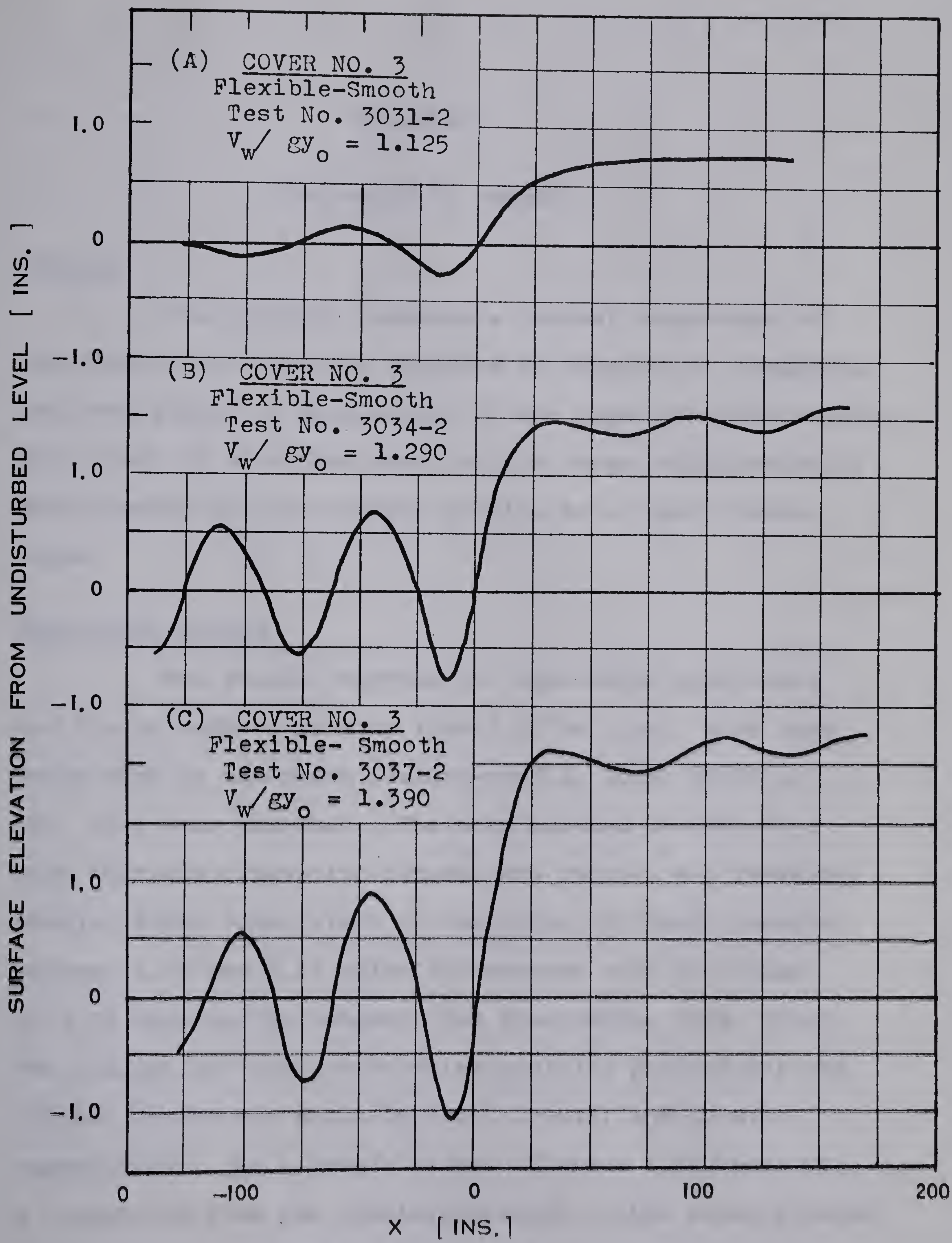

SURFACE PROFILES

FIGURE IV-11

CHAPTER V

DISCUSSION OF RESULTS

5.1 General

This chapter contains a general discussion of the experimental results reported in Chapter IV. Emphasis has been placed on discussing, in the light of these results, the effect of a surface cover on the surge height-velocity relationship and the surface profile of an open channel surge.

5.2 Open-Water Surges

The surges reported for open-water conditions had Froude numbers ranging from 1.07 to 1.58. Over this range, each of the three surface-profile forms shown in FIG. II-1 were observed. The data plotted in FIG. IV-1 show that the transition between the undular and breaking-undular forms takes place in the range of Froude numbers between 1.20 and 1.25 which corresponds with the value of 1.23 observed by Sandover and Zienkiewicz (FIG. II-2). The undular and undular-breaking profiles plotted for the 031-035 Series are shown in FIGs. IV-8(a) and IV-8(b) respectively. At a Froude number of about 1.30 there was a transition from the undular-breaking to the steep-fronted form. However, the steep-fronted surges having Froude

numbers near this value exhibited a subdued and irregular undular form as shown in the profile plotted in FIG. IV-8(c). For classification purposes the dividing line between these two forms was therefore, taken as the point where the ratio between the peak to trough distance of the undulations and the maximum surge height was markedly reduced. The transition based on this criteria can be illustrated by comparing the profiles plotted in FIGs. IV-8(b) and IV-8(c). As Froude number was increased above 1.30, the undulations making up the steep-fronted profile became more subdued finally resulting in the form plotted in FIG. IV-8(d).

The data plotted in the undular range ($V_w/ gy_o < 1.25$) of FIG. IV-1 show a fair correlation with the maximum surge height-velocity relationship obtained experimentally by Sandover and Zienkiewicz (FIG. II-2). In the steep-fronted range of this figure, the plotted points follow a relationship having approximately the same slope as Equation (2-3), however, these points fall somewhat above the plot of this equation.

The average surge height-velocity relationship (η_{ave}/y_o vs. $V_w/\sqrt{gy_o}$) for the open-water data is shown in FIG. IV-2. Throughout the entire range there is a good correlation between the plotted data and the steep-fronted surge equation (Equation 2-3).

5.3 Surface-Profiles for Surges Observed Under Surface Cover Conditions

FIG. V-1 illustrates the surface-profile that was typical of the surges formed under surface cover conditions. This profile has a damped train of waves that develop ahead of the surge front and appear stationary when viewed through a frame of reference travelling with the surge front. The remaining portion of the profile is similar to the steep-fronted form observed under open-water conditions except the slope of the surge front is considerably less for surface cover conditions.

As a surge formed and began to travel through the flume, the waves making up the damped wave-train developed one by one with each new wave having an amplitude slightly less than the one preceeding it. Thus, the number of waves present depends upon the distance the surge has travelled, or in other words, the velocity of propagation of the head of the wave-train is greater than the velocity of propagation of the surge front. In some respects the development of this wave-train is similar to the development of the undular wave-train for open water conditions in that both wave-trains increase their number of waves as the surge travels through the flume and also tend to become damped as distance from the surge front increases. However, the undular wave-train for open water conditions develops behind the surge front, where-as the wave-train for surface cover conditions develops ahead of the surge front.

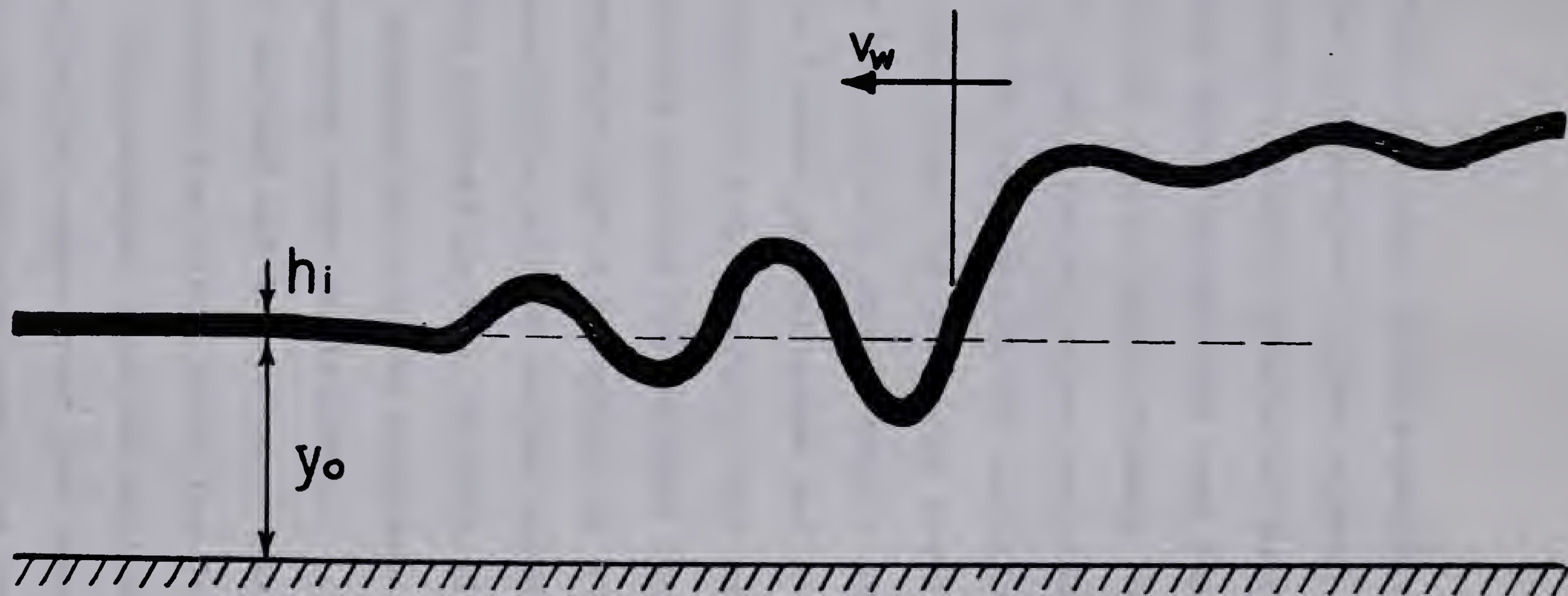

TYPICAL SURGE PROFILE FOR SURFACE COVER CONDITIONS

FIGURE V-1

FIGs. IV-9 and IV-10 demonstrate the effect of surface cover properties on the surface profile. These figures contain a number of plotted surface profiles for surges having approximately the same values of undisturbed depth and Froude number but different surface cover conditions. A comparison of these profiles indicates that the slope of the surface and the wavelength of the undulations that form ahead of the surge front depend on the rigidity of the surface cover, with a greater rigidity resulting in a more gradual slope and a longer wavelength as demonstrated in FIG. IV-9(c). The similarity in the surface profiles plotted for surface cover numbers 1, 3, 4, and 5 indicate that a variation in surface cover roughness or weight has little effect on the surface profile. The open water profile plotted in FIG. IV-9(a) illustrates the radical difference between the surface profiles obtained for open water and surface cover conditions.

A subdued and irregular undular form was observed to develop behind the surge front for Froude numbers greater than 1.20. This undular form was similar to the form observed behind the surge front for open-water steep-fronted surges except that the wavelengths of the undulations were considerably greater for the surface cover case and were approximately equal to the wavelengths found in the wave-train that developed ahead of the surge front. Also, under surface cover conditions this undular form became more

pronounced for increasing Froude numbers whereas the opposite was true for open water surges. FIG. IV-11 shows plots of a number of surface profiles covering a range of Froude numbers and illustrating the development of the undular form behind the surge front.

5.4 Surge Height-Velocity Relationship for Surface Cover Conditions

The dimensional arguments of Section 2.5 resulted in the functional equation:

$$\frac{V_w}{\sqrt{gy_o}} = \text{fn}\left(\frac{\eta}{y_o}, \frac{h_i}{y_o}, \frac{\epsilon_i}{y_o}, \frac{\rho_i}{\rho_w}, \frac{E_i/\rho_i}{gy_o}\right) \quad \ldots\ldots\ldots\ldots \quad (2\text{-}15)$$

In which the non-dimensional parameters ϵ_i/y_o, h_i/y_o, ρ_i/ρ_w and $E_i/\rho_i gy_o$ indicate the possible effect of a surface cover on the relationship between $V_w/\sqrt{gy_o}$ and η/y_o. Of these parameters, ρ_i/ρ_w and h_i/y_o together indicate that the weight of the cover may be relevant, h_i/y_o and $E_i/\rho_i gy_o$ show the possible effect of the rigidity of the surface cover and ϵ_i/y_o represents the possible relevance of surface cover roughness. The purpose of plotting $V_w/\sqrt{gy_o}$ against η_{ave}/y_o in FIGs. IV-3 through IV-7 was to determine the importance of each of these cover properties.

The importance of the relative surface cover roughness ϵ_i/y_o in Equation (2-15) can be determined by examining FIGs. IV-3, IV-5 and IV-7. These figures contain

data representing Covers 1, 3 and 5 in which surface cover roughness was varied whereas weight and rigidity remained practically constant. In general, the data plotted in these figures show a good correlation between Froude number and non-dimensional surge height. Furthermore, an examination of the straight line regression coefficients listed in Table IV-2, for each series of data plotted in the above figures, indicates that there is apparently no systematic pattern of variation in the best fit straight lines. This implies that relative surface cover roughness ϵ_i/y_o was not important to the surge height-velocity relationship over the range of testing and therefore, it can be eliminated from Equation (2-15).

The addition of a uniform surface load on the cover in the case of Cover 4 is equivalent to increasing the cover density ρ_i while leaving its surface roughness and rigidity the same as in Cover 3. The results for these two cover conditions are plotted in FIGs. IV-5 and IV-6. A slight discrepancy in the relationship between $V_w/\sqrt{gy_o}$ and η_{ave}/y_o is apparent in these figures and is verified by the straight line regression coefficients listed in Table IV-2. However, this discrepancy is negligible for all practical purposes in that the relationships followed by the data plotted in these figures are similar enough to suggest that surface cover weight is probably of little importance to the surge height-velocity relationship.

Therefore, if weight is accepted as being unimportant, the parameter ρ_i/ρ_w can also be eliminated from Equation (2-15).

The effect of surface cover rigidity or the parameters h_i/y_o and $E_i/\rho_i g y_o$ can be assessed by comparing data obtained for Covers 2 and 3, since Cover 2 was considerably stiffer than Cover 3 but had approximately the same roughness and weight. Although the data, for Cover 2, plotted in FIG. IV-4 shows considerable scatter (as discussed in Section 4-2), the best fit straight line relationship shows a good correlation with the similar relationship obtained for the data of Cover 3 and plotted in FIG. IV-5. Therefore, the rigidity of the surface cover can be considered unimportant in the surge height-velocity relationship and Equation (2-15) can be reduced to:

$$\frac{V_w}{\sqrt{g y_o}} = fn\left(\frac{\eta}{y_o}\right) \quad \ldots\ldots\ldots\ldots\ldots\ldots \quad (5\text{-}1)$$

for the range in which tests were performed.

A linear regression analysis performed on all of the data plotted in FIGs. IV-3 through IV-7 yielded the expression:

$$\frac{V_w}{\sqrt{g y_o}} = 0.997 + 0.659\,\frac{\eta}{y_o} \quad \ldots\ldots\ldots\ldots\ldots \quad (5\text{-}2)$$

with a correlation coefficient of 0.894 which indicates a good fit and verifies the reduction of Equation (2-15) to Equation (5-1). Equation (2-3) which showed a good

fit to the open water data based on average surge height and Equation (5-2) have been plotted in FIG. V-2. From this figure, it is apparent that the addition of a surface cover results in reduced Froude numbers for a given non-dimensional surge height. The order of magnitude of this reduction is approximately three percent over the range in which data were reported.

In Section 2.4 a celerity equation was derived for idealized surface cover conditions and can be rewritten as:

$$\frac{V_w}{\sqrt{gy_o}} = \left(1 + \frac{3}{2}\frac{\eta}{y_o} + \frac{1}{2}\frac{\eta^2}{y_o^2}\right)^{\frac{1}{2}} \left(1 + \frac{\gamma_i h_i}{\gamma_w y_o}\right)^{\frac{1}{2}} \quad . . . \quad (2\text{-}11)$$

Throughout the testing program, the coefficient $(1 + \gamma_i h_i/\gamma_w y_o)^{\frac{1}{2}}$ had values ranging from 1.040 to 1.107. Equation (2-11) has been plotted in FIG. V-2 for both the maximum and minimum values of this coefficient, $(1 + \gamma_i h_i/\gamma_w y_o)^{\frac{1}{2}}$, thereby forming a band in which the experimental points might theoretically be expected to fall. However, this band indicates that Froude number increases due to the addition of a surface cover for a given value of η/y_o, which is a result opposite to that shown by the experimental evidence. This suggests that the assumptions required for the derivation of Equation (2-11) were not valid.

The Water Resources Branch of the Alberta Department of Agriculture has given the author an opportunity to

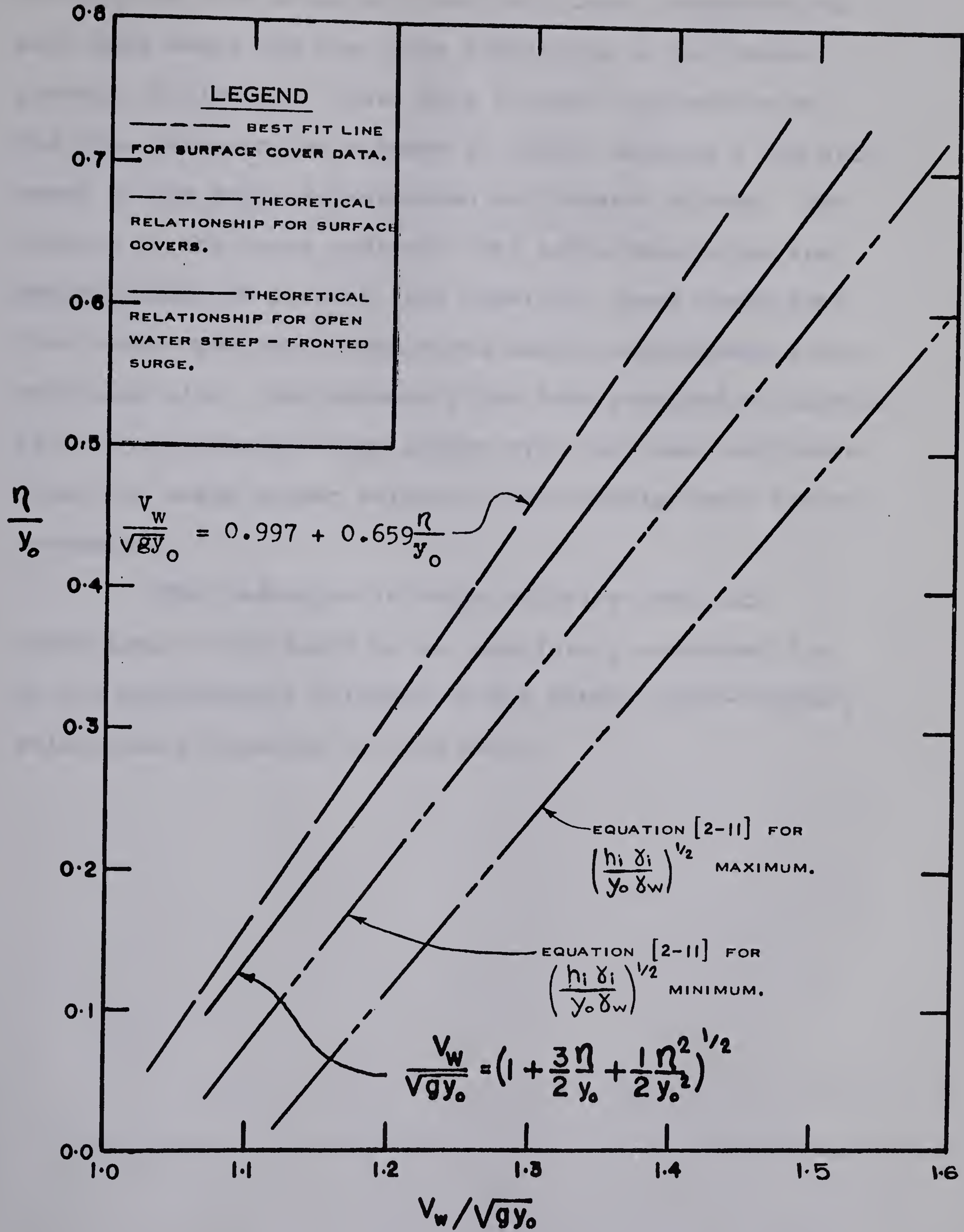

SURGE HEIGHT – VELOCITY RELATIONSHIP

FIGURE V–2

examine the data obtained from field tests conducted for both open water and ice cover conditions on the Brazeau project in Alberta. These data yielded information on the time required for a surge to travel through a 150 mile reach of the North Saskatchewan and Brazeau Rivers. The results of the tests indicate that surge velocities are approximately 30 percent less under ice cover conditions than under open water conditions having approximately the same base flow. Unfortunately the data provided no information on the average surge height over the reach and therefore, the surge height velocity relationship could not be determined.

The reduction in surge velocity under ice conditions in the field is not completely accounted for by the experimental evidence on the surge height-velocity relationship reported in this study.

CHAPTER VI

CONCLUSIONS AND RECOMMENDATIONS

6.1 Conclusions

A review of the literature on the effect of an ice cover on wave motion showed a definite lack of knowledge on the behavior of an open channel surge under ice cover conditions. In the present experimental study, the use of an artificial continuous surface cover having various degrees of structural rigidity constitutes a new approach to the problem.

The test results indicate that a relationship between $V_w/\sqrt{gy_o}$ and η/y_o exists for surface cover conditions as was expected from the dimensional analysis and from the known behavior of open water surges. The results that were obtained under surface cover conditions indicate that the properties of the surface cover have little or no effect on this relationship over the range in which data were obtained.

A comparison of the test data obtained for surface cover and open water conditions shows that the addition of a surface cover results in a slightly reduced surge velocity for a given undisturbed depth and surge height. However, field observations have indicated a greater reduction in

surge velocity under ice conditions that cannot be completely accounted for by the experimental evidence reported herein.

The test results show that a surface cover has a considerable effect on the surface profile of an open channel surge. The undular and undular-breaking forms that are common for open water surges did not occur under surface cover conditions. The surface profiles, observed throughout the entire range of surface cover tests, exhibited a damped train of waves that developed ahead of the surge front. The wavelength associated with these waves was found to depend on the rigidity of the surface cover.

6.2 Recommendations

It is recommended that:

(a) tests be conducted over an extended range of initial conditions and surface cover conditions in an attempt to verify or limit the conclusions of this study;

(b) the effect of a surface cover on friction and ponding behind a surge should be investigated as a possible explanation for the discrepancy between the experimental evidence reported herein and the results of field observations;

(c) the type of surface profile that develops for surface cover conditions should be the subject of further investigation;

(d) tests be carried out for the purpose of finding a

material that can be used in model studies to simulate more closely the properties of an ice cover.

LIST OF REFERENCES

Blench, T., Parallel Development of Open-Channel Flow and Gas Dynamics. ASME-EIC Hydraulics Conference Paper No. 61-EIC-9, 1961.

Benjamin, T.B. and Lighthill, F.R.S., On Cnoidal Waves and Bores. Proceedings of the Royal Society, vol. 224, p. 448, 1954.

Favre, H., Etude des Ondes de Translation. Paris, Dunond, 1935.

Keller, J.B. and Goldstein, E., Water Wave Reflection due to Surface Tension and Floating Ice. Trans. Am. Geophys. Union, vol. 34, n. 1, pp. 43-48, Feb. 1953.

Keulegan, G.H., Wave Motion, chap. II in Hunter Rouse (ed.) "Engineering Hydraulics." John Wiley and Sons Inc., New York, 1949.

Krylov, I͡U.M., Propagation of Long Waves under an Icefield. Trudy Gosudarstuennogo Okeanograficheskogo Instituta, Moscow, No. 8(20), pp. 107-110, 1948.

Lamb, H., Hydrodynamics. Sixth Edition, Cambridge University Press, 1945.

Michel, B., Personal Correspondence. Sept. 27, 1965.

Peters, A.S., The Effect of a Floating Mat on Water Waves. Communication on Pure and Applied Mathematics, vol. 3-174, pp. 319-354, Dec. 1950.

Robin, G. de Q., Wave Propagation through Fields of Pack Ice. Royal Society, Philosophical Transactions, Ser. A, vol. 255, pp. 313-339, 1963.

Sandover, J.A. and Zienkiewicz, O.C., Experiments on Surge Waves. Water Power, vol. 9, p. 418, Nov. 1957.

Shapiro, A. and Simpson, L.S., The Effect of a Broken Icefield on Water Waves. Trans. Am. Geophys. Un. vol. 34, n. 1, pp. 36-42, Feb. 1953.

Shook, G., On Capacitive Pressure Transducers, Report in preparation. Dept. of Civil Engineering, University of Alberta, 1966.

Stoker, J.J., Water Waves. Interscience, New York, 1957.

U. S. Army Corps of Engineers, Bibliography on Snow, Ice, and Permafrost. SIPRE Report 12, vol. VI, n. 7155, Snow, Ice, and Permafrost Research Establishment, Wilmette, Ill.

Weitz, M. and Keller, J.B., The Reflection of Water Waves from Floating Ice in Water of Finite Depth. Communication on Pure and Applied Mathematics, vol. 3, n. 3, pp. 305-318, Sept. 1950.

APPENDIX "A"

DATA PROCESSING

A.1 Calculation of Froude Number and Non-Dimensional Surge Height

The methods used to calculate Froude number and non-dimensional surge heights from the original surge records were somewhat arbitrary and depended largely on the configuration of the surge profile. The following outline demonstrates the steps involved in calculating these two parameters and points out the variation in the methods used for the different surge forms.

a) Undisturbed piezometric depth:

y_p = depth measured on point gauge.

b) Submerged thickness of surface cover:

h_s = value shown in TABLE III-1.

c) Undisturbed depth of water:

$y_o = y_p - h_s$ (for surface cover conditions)

$= y_p$ (for open water conditions)

d) L_{1-2}, L_{2-3} = the distance measured on the surge record representing the time required for the toe of a surge to travel the distance between the two consecutive recording stations indicated by the subscripts. For

the record at each station the toe of the surge was taken as the intersection between the surge front and the undisturbed level. For open water surges this point was difficult to ascertain so the intersection between the undisturbed level and the line having the maximum slope of the surge front was used.

e) Surge velocity at each measuring section:

$$(V_w)_{1,2,3} = \frac{\begin{pmatrix}\text{Speed of the}\\ \text{recorder paper}\end{pmatrix} \times \begin{pmatrix}\text{Distance between}\\ \text{stations}\end{pmatrix}}{(L)_{1,2,3}}$$

$$= \frac{32 \text{ in./min} \quad x \quad 25 \text{ ft.}}{(L)_{1,2,3} \text{ in.} \quad x \quad 60 \text{ sec./ min}}$$

$$= \frac{13.33}{(L)_{1,2,3}} \text{ ft./sec.}$$

where the subscripts 1,2,3 refer to a particular recording station. The values $(L)_{1,2,3}$ are obtained by plotting L_{1-2} and L_{2-3} against distance along the flume and assuming a linear relationship. The plot is then extrapolated or interpolated to give a value of L at each recording station.

f) Froude number = $V_w/\sqrt{gy_o}$

g) Maximum surge height:

η max = The maximum height of the first undulation above the undisturbed level as corrected for gauge factor. η max was determined for open water surges only.

h) Maximum non-dimensional surge height = $\dfrac{\eta_{max}}{y_o}$

i) Average surge height:

(1) Undular and undular-breaking open water surges;

η_{ave} = the average of the maximum height of the first undulation and the height of the first trough above the undisturbed level as corrected for gauge factor.

(2) Surface cover and steep-fronted open water surges;

η_{ave} = the height, above the undisturbed level, of the point of intersection of a curve smoothing the undulations and a straight line having the maximum slope of the surge front as corrected for final gauge factor.

j) Non-dimensional average surge height = $\dfrac{\eta_{ave}}{y_o}$

A.2 Linear Regression

Throughout the analysis of the experimental data the plots of $V_w/\sqrt{gy_o}$ vs η/y_o were fitted with straight lines by the method of least squares.

For a set of n values observed for x and y, the best fit straight line giving a minimum value of the sum of the squares of the error between the observed and predicted values of y is:

$$y = ax + b \qquad \text{(A-1)}$$

where:

$$a = \frac{n \sum_{i=1}^{n}(x_i y_i) - \left(\sum_{i=1}^{n}(x_i)\right)\left(\sum_{i=1}^{n}(y_i)\right)}{n \sum_{i=1}^{n}(x_i)^2 - \left(\sum_{i=1}^{n}(x_i)\right)^2} \quad \text{. . . . . (A-2)}$$

$$b = \frac{\sum_{i=1}^{n}(y_i) - a\sum_{i=1}(x_i)}{n} \quad \text{. . . . . (A-3)}$$

The correlation coefficient for the y on x linear regression is defined as:

$$r^2 = \frac{\left\{n\sum_{i=1} x_i y_i - \left(\sum_{i=1}^{n}(x_i)\right)\left(\sum_{i=1}^{n}(y_i)\right)\right\}^2}{\left\{n\sum_{i=1}^{n}(x_i)^2 - \left(\sum_{i=1}^{n}(x_i)\right)^2\right\}\left\{n\sum_{i=1}^{n}(y_i)^2 - \left(\sum_{i=1}^{n}(y_i)\right)^2\right\}} \quad \text{(A-4)}$$

A.3 Calculation of Surface Profiles

A number of approximate surface profiles were calculated from the original surge records. Since the recorded surge profiles were records of depth at a fixed point against time, these records do not give a true instantaneous surge profile and the validity of the calculated profile depends on the following assumptions:

a) the calculated value for surge velocity is correct for each element of the recorded surge profile at the time it was recorded.

b) the amplitudes shown on the recorded profile are correct for the instant the toe of the surge passes over the recording station.

In determining a surge profile, x' and y

coordinates were measured from an origin at the toe of the surge to a number of points located on the recorded surge profile. The x' coordinates were then converted to x coordinates using the equation:

$$x = \frac{(x')\,(V_W)}{\text{paper speed}} \qquad \text{(A-5)}$$

APPENDIX "B"

THE PROCESSED DATA

TABLE: B-1

PROCESSED DATA - OPEN WATER

TEST NO.	STATION NO.	UNDISTURBED DEPTH y_o (ft.)	L (in.)	V_w $\frac{ft.}{sec.}$	$\frac{V_w}{\sqrt{gy_o}}$	η_{ave} (ft.)	$\frac{\eta_{ave}}{y_o}$	η_{max}	$\frac{\eta_{max}}{y_o}$
021	1	0.196	4.23	3.15	1.250	0.092	0.470	0.061	0.312
(b)*	2	"	4.25	3.14	1.250	0.079	0.403	0.052	0.265
	3	"	4.27	3.13	1.250	0.077	0.394	0.052	0.267
022	1	0.198	3.74	3.56	1.410	0.118	0.596	0.110	0.555
(s)	2	"	3.82	3.50	1.390	0.102	0.515	0.098	0.495
	3	"	3.90	3.42	1.360	0.103	0.520	0.099	0.503
023	1	0.200	3.46	3.86	1.520	0.152	0.762	0.150	0.750
(s)	2	"	3.54	3.77	1.485	0.137	0.688	0.135	0.675
	3	"	3.61	3.70	1.460	0.138	0.692	0.133	0.665
024	1	0.201	3.24	4.11	1.620	0.179	0.890	0.179	0.890
(s)	2	"	3.28	4.06	1.600	0.163	0.810	0.163	0.810
	3	"	3.32	4.02	1.580	0.162	0.806	0.156	0.775
025	1	0.201	3.02	4.42	1.740	0.202	1.000	-	-
(s)	2	"	3.14	4.25	1.675	0.180	0.896	-	-
	3	"	3.24	4.11	1.620	0.175	0.870	-	-
031	1	0.303	3.78	3.52	1.130	0.075	0.249	0.057	0.190
(u)	2	"	3.76	3.54	1.135	0.078	0.256	0.054	0.178
	3	"	3.74	3.56	1.140	0.077	0.255	0.054	0.178
032b	1	0.298	3.38	3.94	1.270	0.136	0.456	0.092	0.308
(b)	2	"	3.42	3.90	1.260	0.132	0.443	0.088	0.294
	3	"	3.46	3.85	1.240	0.120	0.404	0.084	0.283

*u, b, s denote undular, undular breaking, and steep-fronted surge forms respectively.

TABLE: B-1 (continued)

TEST NO.	STATION NO.	UNDISTURBED DEPTH y_o (ft.)	L (in.)	V_w $\frac{ft.}{sec.}$	$\frac{V_w}{\sqrt{gy_o}}$	η_{ave} (ft.)	$\frac{\eta_{ave}}{y_o}$	η_{max} (ft.)	$\frac{\eta_{max}}{y_o}$
033	1	0.305	3.20	4.17	1.335	0.157	0.515	0.143	0.469
(s)	2	"	3.22	4.14	1.325	0.150	0.492	0.134	0.440
	3	"	3.24	4.12	1.315	0.145	0.476	0.126	0.413
034	1	0.296	3.01	4.43	1.435	0.184	0.622	0.179	0.605
(s)	2	"	3.07	4.34	1.400	0.174	0.588	0.167	0.565
	3	"	3.12	4.27	1.380	0.166	0.561	0.157	0.530
035	1	0.297	2.88	4.63	1.500	0.204	0.688	0.202	0.680
(s)	2	"	2.94	4.53	1.465	0.192	0.647	0.184	0.620
	3	"	3.00	4.45	1.440	0.179	0.603	0.167	0.560
041	1	0.403	3.45	3.86	1.070	0.064	0.160	0.055	0.137
(u)	2	"	3.39	3.93	1.090	0.070	0.174	0.054	0.135
	3	"	3.32	4.02	1.115	0.072	0.177	0.053	0.132
042	1	0.400	3.15	4.23	1.180	0.141	0.352	0.105	0.262
(u)	2	"	3.13	4.25	1.185	0.136	0.340	0.093	0.234
	3	"	3.12	4.27	1.190	0.138	0.347	0.094	0.235
043	1	0.397	2.94	4.53	1.260	0.193	0.486	0.136	0.343
(b)	2	"	2.94	4.53	1.260	0.183	0.462	0.121	0.304
	3	"	2.94	4.53	1.260	0.182	0.459	0.121	0.304
044	1	0.405	2.84	4.69	1.310	0.190	0.468	0.179	0.442
(s)	2	"	2.84	4.69	1.310	0.181	0.455	0.163	0.403
	3	"	2.84	4.69	1.310	0.193	0.476	0.170	0.420
045	1	0.400	2.78	4.80	1.340	0.221	0.552	0.212	0.530
(s)	2	"	2.78	4.80	1.340	0.206	0.505	0.192	0.480
	3	"	2.78	4.80	1.340	0.221	0.515	0.188	0.470

TABLE: B-2

PROCESSED DATA - COVER NO. 1

TEST NO.	STATION NO.	UNDISTURBED DEPTH y_o (ft.)	L (in.)	V_w ft./sec.	$\frac{V_w}{\sqrt{gy_o}}$	η_{ave} x 10^{+1} (ft.)	$\frac{\eta_{ave}}{y_o}$
1021	1	0.174	4.46	2.99	1.260	0.734	0.421
	2	"	4.58	2.91	1.230	0.650	0.374
	3	"	4.70	2.84	1.200	0.583	0.335
1022	1	0.170	4.11	3.25	1.390	1.200	0.706
	2	"	4.17	3.20	1.370	1.010	0.594
	3	"	4.23	3.15	1.345	0.875	0.515
1023	1	0.170	3.75	3.56	1.520	1.530	0.900
	2	"	3.85	3.46	1.480	1.380	0.812
	3	"	3.95	3.38	1.445	1.180	0.694
1024	1	0.169	3.46	3.86	1.660	1.810	1.070
	2	"	3.60	3.70	1.590	1.610	0.953
	3	"	3.74	3.57	1.530	1.450	0.858
1231	1	0.269	3.99	3.34	1.135	0.666	0.247
	2	"	3.99	3.34	1.135	0.583	0.217
	3	"	3.99	3.34	1.335	0.583	0.217
1232	1	0.268	3.61	3.70	1.260	1.120	0.418
	2	"	3.63	3.68	1.250	1.000	0.373
	3	"	3.65	3.66	1.245	0.942	0.352
1233	1	0.269	3.38	3.95	1.345	1.540	0.573
	2	"	3.42	3.90	1.330	1.375	0.511
	3	"	3.46	3.86	1.310	1.290	0.480
1234	1	0.269	3.19	4.18	1.420	1.920	0.715
	2	"	3.25	4.11	1.400	1.670	0.620
	3	"	3.31	4.03	1.375	1.500	0.558
1041	1	0.369	3.61	3.70	1.075	0.625	0.169
	2	"	3.59	3.72	1.080	0.541	0.147
	3	"	3.57	3.74	1.085	0.533	0.145
1042	1	0.372	3.30	4.05	1.170	1.070	0.288
	2	"	3.30	4.05	1.170	0.983	0.264
	3	"	3.30	4.05	1.170	1.000	0.269
1043	1	0.365	3.13	4.27	1.245	1.500	0.411
	2	"	3.12	4.27	1.245	1.280	0.350
	3	"	3.12	4.27	1.245	1.290	0.353

TABLE: B-2 (continued)

TEST NO.	STATION NO.	UNDISTURBED DEPTH y_o (ft.)	L (in.)	V_w $\frac{ft.}{sec.}$	$\frac{V_w}{\sqrt{gy_o}}$	$\eta_{ave} \times 10^{+1}$ (ft.)	$\frac{\eta_{ave}}{y_o}$
1044	1	0.364	3.03	4.40	1.285	1.920	0.524
	2	"	3.01	4.43	1.295	1.650	0.453
	3	"	2.99	4.46	1.305	1.600	0.440

TABLE: B-3

PROCESSED DATA - COVER NO. 2

TEST NO.	STATION NO.	UNDISTURBED DEPTH y_o (ft.)	L (in.)	V_w $\frac{ft.}{sec.}$	$\frac{V_w}{\sqrt{gy_o}}$	η ave x 10^{+1} (ft.)	$\frac{\eta\ ave}{y_o}$
2121	1	0.172	5.20	2.56	1.090	0.306	0.178
	2	"	5.16	2.58	1.100	0.302	0.176
	3	"	5.12	2.61	1.110	0.309	0.180
2122	1	0.171	4.74	2.81	1.195	0.569	0.333
	2	"	4.68	2.85	1.215	0.540	0.316
	3	"	4.62	2.89	1.230	0.500	0.292
2123	1	0.168	4.64	2.87	1.230	0.735	0.437
	2	"	4.58	2.91	1.250	0.635	0.378
	3	"	4.52	2.95	1.265	0.454	0.270
2124	1	0.173	4.42	3.02	1.280	0.875	0.505
	2	"	4.34	3.07	1.300	0.715	0.413
	3	"	4.26	3.13	1.325	0.545	0.315
2125	1	0.167	4.22	3.16	1.360	1.050	0.630
	2	"	4.22	3.16	1.360	0.873	0.523
	3	"	4.22	3.16	1.360	0.773	0.462
2331	1	0.268	4.14	3.22	1.095	0.323	0.120
	2	"	4.14	3.22	1.095	0.358	0.133
	3	"	4.14	3.22	1.095	0.390	0.145
2332 (b)	1	0.271	4.09	3.26	1.105	0.533	0.197
	2	"	3.99	3.34	1.130	0.549	0.202
	3	"	3.89	3.43	1.160	0.597	0.220
2333	1	0.266	3.93	3.39	1.160	0.808	0.304
	2	"	3.83	3.48	1.190	0.796	0.299
	3	"	3.73	3.58	1.220	0.780	0.293
2334	1	0.271	3.84	3.48	1.180	0.930	0.343
	2	"	3.66	3.65	1.240	0.916	0.338
	3	"	3.48	3.83	1.300	0.866	0.320
2335	1	0.266	3.68	3.63	1.240	1.230	0.463
	2	"	3.56	3.75	1.280	1.115	0.420
	3	"	3.44	3.88	1.320	1.070	0.403
2336	1	0.269	3.46	3.86	1.315	1.370	0.510
	2	"	3.44	3.88	1.320	1.230	0.458
	3	"	3.42	3.90	1.325	1.080	0.440

TABLE: B-3 (continued)

TEST NO.	STATION NO.	UNDISTURBED DEPTH y_o (ft.)	L (in.)	V_w $\frac{ft.}{sec.}$	$\frac{V_w}{\sqrt{gy_o}}$	η_{ave} x 10^{+1} (ft.)	$\frac{\eta_{ave}}{y_o}$
2337	1	0.267	3.38	3.94	1.345	1.550	0.580
	2	"	3.31	4.03	1.375	1.390	0.521
	3	"	3.25	4.10	1.400	1.300	0.487
2338	1	0.268	3.27	4.08	1.390	1.700	0.635
	2	"	3.21	4.16	1.420	1.550	0.578
	3	"	3.15	4.23	1.440	1.450	0.541
2141	1	0.366	3.71	3.60	1.050	0.488	0.133
	2	"	3.61	3.70	1.080	0.458	0.125
	3	"	3.51	3.80	1.110	0.435	0.119
2142	1	0.368	3.46	3.85	1.120	0.688	0.187
	2	"	3.42	3.90	1.135	0.800	0.217
	3	"	3.38	3.95	1.150	0.712	0.194
2143	1	0.369	3.47	3.84	1.115	0.930	0.252
	2	"	3.33	4.01	1.160	1.000	0.271
	3	"	3.19	4.18	1.215	0.950	0.258
2194	1	0.367	3.35	3.98	1.155	1.100	0.300
	2	"	3.21	4.16	1.210	1.080	0.294
	3	"	3.07	4.34	1.260	1.110	0.302
2145	1	0.369	3.35	3.98	1.155	1.260	0.342
	2	"	3.15	4.23	1.230	1.290	0.350
	3	"	2.95	4.52	1.310	1.270	0.344
2146	1	0.364	3.27	4.08	1.195	1.330	0.366
	2	"	3.09	4.32	1.260	1.330	0.366
	3	"	2.91	4.58	1.340	1.270	0.349
2147	1	0.369	3.18	4.20	1.220	1.580	0.428
	2	"	3.00	4.45	1.290	1.625	0.440
	3	"	2.82	4.73	1.370	1.420	0.385
2148	1	0.369	3.03	4.40	1.275	1.650	0.447
	2	"	2.93	4.55	1.320	1.670	0.453
	3	"	2.84	4.70	1.360	1.420	0.385

TABLE: B-4

PROCESSED DATA - COVER NO. 3

TEST NO.	STATION NO.	UNDISTURBED DEPTH y_o (ft.)	L (in.)	V_w $\frac{ft.}{sec.}$	$\frac{V_w}{\sqrt{gy_o}}$	η_{ave} x 10^{+1}	$\frac{\eta_{ave}}{y_o}$
3021	1	0.170	5.01	2.66	1.135	0.366	0.215
	2	"	4.99	2.67	1.140	0.382	0.225
	3	"	4.97	2.68	1.145	0.422	0.248
3022	1	0.173	4.46	2.99	1.265	0.636	0.368
	2	"	4.56	2.92	1.240	0.569	0.329
	3	"	4.66	2.86	1.210	0.560	0.324
3023	1	0.171	4.27	3.12	1.330	0.858	0.502
	2	"	4.37	3.05	1.300	0.796	0.466
	3	"	4.47	2.98	1.270	0.812	0.475
3024	1	0.171	4.07	3.28	1.395	1.070	0.625
	2	"	4.19	3.19	1.360	0.935	0.547
	3	"	4.31	3.10	1.320	0.853	0.498
3025	1	0.169	3.93	3.39	1.455	1.170	0.692
	2	"	4.07	3.28	1.410	1.080	0.639
	3	"	4.21	3.17	1.360	1.030	0.610
3026	1	0.171	3.82	3.49	1.485	1.390	0.813
	2	"	3.89	3.43	1.460	1.160	0.678
	3	"	3.96	3.37	1.435	1.110	0.650
3027	1	0.169	3.62	3.68	1.580	1.590	0.940
	2	"	3.74	3.57	1.530	1.220	0.722
	3	"	3.86	3.46	1.485	1.340	0.793
3031	1	0.268	4.13	3.23	1.100	0.616	0.230
	2	"	4.03	3.31	1.125	0.577	0.215
	3	"	3.93	3.39	1.150	0.577	0.215
3032	1	0.267	3.87	3.45	1.180	0.808	0.302
	2	"	3.85	3.46	1.180	0.783	0.294
	3	"	3.83	3.48	1.185	0.717	0.268
3033	1	0.267	3.67	3.63	1.240	1.000	0.375
	2	"	3.69	3.62	1.235	0.940	0.352
	3	"	3.71	3.60	1.230	0.907	0.340
3034	1	0.265	3.49	3.82	1.310	1.250	0.472
	2	"	3.55	3.76	1.290	1.150	0.434
	3	"	3.61	3.70	1.265	1.050	0.396

TABLE: B-4 (continued)

TEST NO.	STATION NO.	UNDISTURBED DEPTH y_o (ft.)	L (in.)	V_w $\frac{ft.}{sec.}$	$\frac{V_w}{\sqrt{gy_o}}$	$\eta_{ave} \times 10^{+1}$ (ft.)	$\frac{\eta_{ave}}{y_o}$
3035	1	0.267	3.40	3.92	1.340	1.375	0.515
	2	"	3.44	3.88	1.325	1.340	0.502
	3	"	3.48	3.83	1.310	1.180	0.442
3036	1	0.272	3.29	4.05	1.390	1.580	0.581
	2	"	3.33	4.01	1.375	1.520	0.559
	3	"	3.36	3.97	1.360	1.360	0.500
3037	1	0.272	3.20	4.17	1.410	1.750	0.643
	2	"	3.25	4.11	1.390	1.670	0.615
	3	"	3.30	4.04	1.365	1.480	0.544
3042	1	0.367	3.42	3.90	1.135	0.800	0.218
	2	"	3.42	3.90	1.135	0.833	0.227
	3	"	3.42	3.90	1.135	0.760	0.207
3043	1	0.367	3.26	4.09	1.190	1.000	0.272
	2	"	3.30	4.04	1.175	0.990	0.270
	3	"	3.34	3.99	1.160	0.932	0.254
3044	1	0.364	3.15	4.23	1.235	1.170	0.322
	2	"	3.21	4.15	1.210	1.200	0.330
	3	"	3.27	4.08	1.190	1.030	0.283
3045	1	0.369	3.07	4.35	1.260	1.390	0.377
	2	"	3.11	4.29	1.245	1.380	0.374
	3	"	3.15	4.23	1.230	1.240	0.366
3046	1	0.369	3.02	4.42	1.280	1.530	0.415
	2	"	3.05	4.37	1.265	1.550	0.420
	3	"	3.09	4.32	1.250	1.320	0.358
3047	1	0.366	3.00	4.45	1.300	1.670	0.456
	2	"	3.00	4.45	1.300	1.680	0.459
	3	"	3.00	4.45	1.300	1.510	0.413
3048	1	0.370	2.88	4.63	1.345	1.920	0.520
	2	"	2.90	4.60	1.335	1.930	0.522
	3	"	2.92	4.37	1.325	1.710	0.462

TABLE: B-5

PROCESSED DATA - COVER NO. 4

TEST NO.	STATION NO.	UNDISTURBED DEPTH y_o (ft.)	L (in.)	V_w $\frac{ft.}{sec.}$	$\frac{V_w}{\sqrt{gy_o}}$	η ave x 10^{+1} (ft.)	$\frac{\eta \text{ ave}}{y_o}$
4021	1	0.159	5.11	2.61	1.155	0.448	0.282
	2	"	5.13	2.60	1.150	0.433	0.272
	3	"	5.15	2.59	1.145	0.417	0.262
4022	1	0.158	4.65	2.87	1.270	0.664	0.420
	2	"	4.79	2.79	1.235	0.591	0.374
	3	"	4.93	2.71	1.200	0.542	0.343
4023	1	0.166	4.35	3.07	1.330	0.862	0.520
	2	"	4.45	3.00	1.300	0.750	0.452
	3	"	4.55	2.93	1.270	0.708	0.426
4024	1	0.160	4.15	3.22	1.420	1.080	0.675
	2	"	4.29	3.11	1.370	0.916	0.572
	3	"	4.43	3.01	1.325	0.833	0.520
4025	1	0.163	3.92	3.40	1.490	1.320	0.810
	2	"	4.02	3.32	1.455	1.040	0.638
	3	"	4.12	3.24	1.420	0.983	0.603
4026	1	0.163	3.72	3.59	1.570	1.570	0.962
	2	"	3.84	3.48	1.520	1.250	0.768
	3	"	3.96	3.37	1.470	1.150	0.705
4031	1	0.260	4.27	3.12	1.080	0.362	0.139
	2	"	4.37	3.05	1.055	0.350	0.135
	3	"	4.47	3.98	1.030	0.325	0.125
4032	1	0.259	4.07	3.28	1.140	0.647	0.250
	2	"	4.09	3.26	1.130	0.600	0.232
	3	"	4.11	3.24	1.125	0.575	0.222
4033	1	0.257	3.87	3.45	1.200	0.854	0.320
	2	"	3.91	3.41	1.185	0.792	0.297
	3	"	3.95	3.38	1.175	0.708	0.265
4034	1	0.261	3.68	3.62	1.250	1.020	0.390
	2	"	3.74	3.57	1.230	0.950	0.364
	3	"	3.80	3.51	1.210	0.833	0.319
4035	1	0.261	3.57	3.74	1.290	1.210	0.464
	2	"	3.61	3.70	1.275	1.100	0.421
	3	"	3.65	3.66	1.265	1.000	0.383

TABLE: B-5 (continued)

TEST NO.	STATION NO.	UNDISTURBED DEPTH y_o (ft.)	L (in.)	V_w $\frac{ft.}{sec.}$	$\frac{V_w}{\sqrt{gy_o}}$	η ave x 10^{+1} (ft.)	$\frac{\eta \text{ ave}}{y_o}$
4036	1	0.264	3.46	3.85	1.320	1.340	0.507
	2	"	3.50	3.81	1.305	1.250	0.473
	3	"	3.54	3.77	1.290	1.080	0.409
4037	1	0.261	3.30	4.04	1.395	1.530	0.586
	2	"	3.36	3.97	1.370	1.440	0.551
	3	"	3.42	3.90	1.345	1.230	0.471
4038	1	0.256	3.15	4.23	1.475	1.900	0.742
	2	"	3.21	4.16	1.450	1.625	0.635
	3	"	3.27	4.08	1.425	1.500	0.586
4041	1	0.359	3.63	3.68	1.080	0.583	0.162
	2	"	3.63	3.68	1.080	0.550	0.153
	3	"	3.63	3.68	1.080	0.534	0.149
4042	1	0.362	3.49	3.82	1.120	0.842	0.233
	2	"	3.51	3.80	1.115	0.800	0.221
	3	"	3.53	3.78	1.100	0.768	0.212
4043	1	0.365	3.38	3.95	1.150	1.040	0.285
	2	"	3.38	3.95	1.150	1.000	0.274
	3	"	3.38	3.95	1.150	0.913	0.250
4044	1	0.361	3.25	4.10	1.200	1.230	0.341
	2	"	3.27	4.08	1.195	1.160	0.321
	3	"	3.29	4.05	1.190	1.060	0.294
4045	1	0.362	3.15	5.23	1.240	1.420	0.392
	2	"	3.17	5.21	1.235	1.320	0.365
	3	"	3.19	5.18	1.225	1.210	0.334
4046	1	0.354	3.07	4.34	1.285	1.650	0.467
	2	"	3.09	4.32	1.275	1.480	0.418
	3	"	3.11	4.29	1.265	1.370	0.387
4047	1	0.356	2.96	4.51	1.330	1.920	0.540
	2	"	2.96	4.51	1.330	1.730	0.486
	3	"	2.96	4.51	1.330	1.630	0.458

TABLE: B-6

PROCESSED DATA - COVER NO. 5

TEST NO.	STATION NO.	UNDISTURBED DEPTH y_o (ft.)	L (in.)	V_w $\frac{ft.}{sec.}$	$\frac{V_w}{\sqrt{gy_o}}$	$\eta_{ave} \times 10^{+1}$ (ft.)	$\frac{\eta_{ave}}{y_o}$
5021	1	0.159	5.10	2.61	1.155	0.326	0.205
	2	"	5.20	2.56	1.130	0.350	0.220
	3	"	5.30	2.52	1.115	0.294	0.248
5022	1	0.159	4.60	2.90	1.280	0.636	0.400
	2	"	4.82	2.77	1.225	0.592	0.372
	3	"	5.04	2.65	1.170	0.484	0.304
5023	1	0.156	4.22	3.16	1.410	0.992	0.636
	2	"	4.42	3.02	1.350	0.875	0.561
	3	"	4.62	2.89	1.290	0.754	0.483
5024	1	0.157	3.89	3.43	1.525	1.280	0.815
	2	"	4.11	3.24	1.440	1.120	0.713
	3	"	4.33	3.08	1.370	0.937	0.596
5025	1	0.158	3.61	3.70	1.640	1.550	0.980
	2	"	3.85	3.46	1.530	1.375	0.870
	3	"	4.09	3.26	1.440	1.220	0.772
5031	1	0.287	4.10	3.25	1.130	0.581	0.227
	2	"	4.10	3.25	1.130	0.541	0.212
	3	"	4.10	3.25	1.130	0.595	0.232
5032	1	0.285	3.79	3.52	1.235	0.930	0.364
	2	"	3.81	3.50	1.230	0.875	0.343
	3	"	3.83	3.48	1.220	0.833	0.327
5033	1	0.288	3.48	3.83	1.330	1.200	0.465
	2	"	3.56	3.74	1.300	1.220	0.473
	3	"	3.64	3.66	1.270	1.055	0.408
5034	1	0.286	3.33	4.01	1.405	1.600	0.630
	2	"	3.41	4.91	1.365	1.450	0.572
	3	"	3.49	4.82	1.335	1.350	0.532
5035	1	0.289	3.16	4.22	1.460	1.900	0.730
	2	"	3.24	4.12	1.425	1.530	0.590
	3	"	3.32	4.02	1.390	1.490	0.573
5041	1	0.358	3.53	3.78	1.110	0.558	0.156
(b)	2	"	3.63	3.68	1.080	0.542	0.151
	3	"	3.73	3.58	1.050	0.492	0.137

TABLE: B-6 (continued)

TEST NO.	STATION NO.	UNDISTURBED DEPTH y_o (ft.)	L (in.)	V_w $\frac{ft.}{sec.}$	$\frac{V_w}{\sqrt{gy_o}}$	$\eta_{ave} \times 10^{+1}$ (ft.)	$\frac{\eta_{ave}}{y_o}$
5042	1	0.352	3.34	4.00	1.190	0.907	0.258
	2	"	3.38	3.95	1.170	0.908	0.258
	3	"	3.42	3.90	1.160	0.842	0.239
5043	1	0.353	3.13	4.27	1.270	1.300	0.369
	2	"	3.21	4.16	1.235	1.310	0.372
	3	"	3.29	4.06	1.205	1.110	0.313
5044	1	0.359	2.98	4.48	1.320	1.630	0.455
	2	"	3.06	4.36	1.280	1.525	0.425
	3	"	3.14	4.25	1.250	1.410	0.393
5045	1	0.351	2.93	4.55	1.355	1.830	0.521
	2	"	2.99	4.46	1.330	1.750	0.498
	3	"	3.05	4.37	1.300	1.600	0.456